Climate Change Impacts on Net Primary Production (NPP) and Export Production (EP) Regulated by Increasing Stratification and Phytoplankton Community Structure in the CMIP5 Models

Weiwei Fu, James Randerson and J. Keith Moore

Department of Earth System Science, University of California, Irvine, California, USA, 92697

Abstract

We examine climate change impacts on net primary production (NPP) and export production (sinking particulate flux; EP) with simulations from nine Earth System Models (ESMs) performed in the framework of the fifth Coupled Model Inter-comparison Project (CMIP5). Global NPP and EP are reduced by the end of the century for the intense warming scenario of Representative Concentration Pathway (RCP) 8.5. Relative to the 1990s, NPP in the 2090s is reduced by 2.3-16% and EP by 7-18%. The models with the largest increases in stratification (and largest relative declines in NPP and EP) also show the largest positive biases in stratification for the contemporary period, suggesting some overestimation of climate change impacts on NPP and EP. All of the CMIP5 models show an increase in stratification in response to surface-ocean warming and freshening, which is accompanied by decreases in surface nutrients, NPP, and EP.

There is considerable variability across the models in the magnitudes of NPP, EP, surface nutrient concentrations, and their perturbations by climate change. The negative response of NPP and EP to increasing stratification reflects primarily a bottom-up control, as upward nutrient flux declines at the global scale. Models with dynamic phytoplankton community structure show larger declines in EP than in NPP. This pattern is driven by phytoplankton community composition shifts, with reductions in productivity by large phytoplankton as smaller phytoplankton (which export less efficiently) are favored under the increasing nutrient stress. Thus, the projections of the NPP response to climate change are critically dependent on the simulated phytoplankton community structure, the efficiency of the biological pump, and the resulting levels of regenerated production, which vary widely across the models. Community structure is represented simply in the CMIP5 models, and should be expanded

and improved to better capture the spatial patterns and changes in export efficiency that seem necessary for predicting climate change impacts on NPP.

1 Introduction

Ocean net primary production (NPP) and particulate organic carbon export (EP) are key elements of marine biogeochemistry and are influenced by the ongoing climate change due to rising concentrations of atmospheric CO_2 and other greenhouse gases. Ocean warming has increasing impacts on ocean ecosystems by modifying the ecophysiology and distribution of marine organisms, and by altering ocean circulation and stratification. Ocean ecosystems also are important components of the climate system, influencing the atmospheric abundance of radiative agents such as CO_2, N_2O, aerosols and the bio-optical properties of seawater and upper ocean physics (Bopp et al. 2013; Goldstein et al. 2003; Manizza et al. 2008; Schmittner and Galbraith 2008; Siegenthaler and Wenk 1984). Therefore, understanding the mechanisms controlling NPP and EP is essential for understanding the global cycles of carbon and other bioactive elements, and their links to climate. (Passow and Carlson 2012).

Upper ocean stratification plays a key role in ocean biogeochemical processes. In particular, mixed layer depth (MLD) regulates the interplay between light availability for photosynthesis (Hannon et al. 2001) and nutrient supply to the upper ocean (e.g., Pollard et al. 2009). Upper ocean stratification is defined here as the density difference between the surface and 200 m depth (Capotondi et al. 2012), which is indicative of the degree of coupling and nutrient fluxes between the euphotic zone and the ocean interior. The density gradient at the base of the mixed layer affects entrainment processes, which play a crucial role in mixed layer deepening and in particle sinking/export from the euphotic zone. Stratification can also influence ocean ventilation (Luo et al. 2009), which has important consequences for oceanic uptake of carbon and oxygen. Thus, changes in stratification over the remainder of the 21st century have the potential to influence NPP and EP across marine ecosystems.

Stratification tends to increase in response to ocean surface warming and freshening in 21st century climate change simulations. Increased stratification reduces the input of sub-surface nutrients to the euphotic zone and can lead to decreasing NPP and EP through increasing nutrient limitation. Many studies have suggested decreases in global NPP and EP over the 21 century using models with varying degrees of complexity (Bopp et al. 2001; Cabré et al. 2015; Dutkiewicz et al. 2013; Froelicher et al. 2009; Fung et al. 2005; Plattner et al. 2001; Schmittner et al. 2008). For the RCP8.5 scenario, CMIP5 ESM estimates of changes in export production range from −7 to −18% relative to 1990s and for NPP these changes range from −2 to −16% (Bopp et al. 2013).

The relative importance of different ecological controls on NPP and EP depends, in part, on an individual model's capacity to represent plankton functional types (PFT) (Jin et al. 2006; Le Quere et al. 2005) and their unique physiological and ecological characteristics, which determine how efficiently they are exported from surface waters. Increasing nutrient stress can shift phytoplankton community composition, favoring smaller phytoplankton, which are more efficient at nutrient uptake, over larger phytoplankton (Bopp et al. 2001; Steinacher et al. 2010; Vichi et al. 2011). These community shifts can modify the efficiency of carbon export to the interior ocean. However, the treatment of plankton communities is relatively simple in the CMIP5 models, with 1-3 phytoplankton functional types and typically one zooplankton group (Bopp et al. 2013).

Several previous studies have studied the biogeochemical response to climate change in the CMIP5 models. Bopp et al. (2013) examined output from 10

CMIP5 models emphasizing model mean biogeochemical responses to multiple stressors and trends over the 21st century relative to 1990s means for each model (also applying a correction for long-term trends in model output). Cabré et al. (2015) also analyzed the CMIP5 models examining changes between model output averaged over the period 1980-1999 with years 2080-2099. This study broke down the global output into different ocean biomes for analysis. Laufkötter et al. (2015a) also analyzed output from nine coupled climate-carbon ESMs including many of the CMIP5 models to study how climate change processes impact NPP comparing two twenty-year periods (2012-2031 and 2081-2100). They suggested strong roles for temperature and top-down grazing control in driving the NPP response, particularly at lower latitudes. Both Cabré et al. (2015) and Laufkötter et al. (2015) conclude that changing light levels were not a primary driver of changes in NPP except at the highest latitudes where there were strong changes in sea ice cover. Thus, we do not consider light effects in this work, where our focus is on the global-scale. More detailed regional studies of the CMIP5 model output have been carried out for the Arctic Ocean (Vancoppenolle et al., 2013) and the Southern Ocean (Leung et al., 2015; Hauck et al., 2015; and Ito et al., 2015).

We analyzed centennial-scale changes in NPP and EP in response to increasing surface stratification and other physical factors. We use historical (1850-2005) and Representative Concentration Pathway (RCP) 8.5 (2006-2100) ESM simulations from the fifth phase of the Coupled Model Inter-comparison Project (CMIP5). One goal of this study is to study long-term trends in NPP and EP under strong warming conditions to identify the mechanisms behind these changes, including the physical factors that regulate nutrient availability. We also examined variability in NPP, EP, and surface nutrient concentrations across the models, to highlight some of the large differences and uncertainties in the projections of climate change impacts on marine biogeochemistry.

2 Methods

We analyzed simulations from a set of 9 ESMs that contributed output to the Earth System Grid Federation as a part of CMIP5 (Taylor et al. 2012). Required physical ocean variables were temperature, salinity, and potential density; required biogeochemistry variables were macro-nutrients (nitrate, phosphate, and silicic acid), iron, chlorophyll, NPP and EP. The selection of the 9 models investigated here (Table 1) was based on the availability of these variables.

The historical and RCP8.5 simulations we analyzed had prescribed atmospheric CO_2 mole fractions and forcing from other greenhouse gases and aerosols, anthropogenic land use, and solar variability. Volcanic forcing also was included during the historical period. The RCP 8.5 is a strong warming scenario with an increase in radiative forcing of 8.5 W/m^2 by 2100 as atmospheric CO_2 mole fractions reach 936 ppm (Moss et al. 2010; van Vuuren et al. 2011). In the case where several ensemble members were available from an individual ESM, we analyzed only the first member.

A simple description of the 9 ESMs is presented in Tables 1 and 2. Atmospheric and ocean resolutions vary across the models (Table 1). Typical atmospheric horizontal grid resolution is ~2°, but it ranges from 0.94 to 3.8°. Typical ocean horizontal resolution is ~1°, ranging from 0.3° to 2°. In the vertical, there are 24 to 95 levels in the atmosphere and 31 to 63 levels in the ocean. All marine biogeochemical components are nutrient–phytoplankton–zooplankton–detritus (NPZD) models, but with varying degrees of complexity, illustrated for instance by the number of phytoplankton functional groups (from 1 to 3) or limiting nutrients (from 3 to 5) that are explicitly represented (Table 2).

In our analysis, we used the CMIP5 variable denoting the vertical integration of NPP and sinking export of organic particles at 100 m (EP). We present global mean estimates as the area-weighted or volume-weighted mean by the grid-cell area/volume from an individual model. Monthly mean data are averaged to obtain annual means and the annual mean data are interpolated onto a common 1°×1° regular grid for the comparison of the 2-D fields.

3 Results

3.1 Stratification changes

Stratification, defined here as the density difference between the depth of 200 m and the surface, is a useful indicator of change in the upper ocean, as it integrates changes in both temperature and salinity. In Figure 1a, we present the time series of global mean stratification changes for the historical period and the RCP8.5 projection. All the models project an increase in stratification (ranging from 6% to 30% at 2100). However, the amplitude of stratification differs considerably across the models. The GFDL-ESM2M and MPI models are relatively close to the observed mean stratification in the WOA09 dataset (red square, 1.81 kg/m^3) for the present era. NorESM1-ME shows the weakest stratification (1.74 kg/m^3) while the stratification in HadGEM2-ES is strongest (2.45 kg/m^3). Long-term trends are in general agreement across models, but the rate of stratification increase varies, with IPSL-CM5A-MR showing a more rapid increase while NorESM1-ME has the slowest increase in stratification.

Surface processes that decrease density can largely explain the stratification increase in the RCP8.5 projections. Global mean sea surface temperature (SST) warms by 2.6-3.5°C, accompanied by sea surface salinity (SSS) decreases of 0.05-0.25 psu over the 21st century (Figure 1). By 2100, the global mean SST ranges from 20.4°C (HadGEM2-ES) to 21.8°C (NorESM1-ME). Model spread decreases in the RCP8.5 projections in response to strong anthropogenic forcing (Figure 1b). The SSS shows a clear declining tendency from 1850 to 2100 (Figure 1). Compared to the WOA09 observational data, most of the models are too fresh at the surface in the 1990s, especially the HadGEM2-ES, which has the lowest global mean SSS. The model spread is partly due to internal variability simulated by the climate models. Model differences in spin up procedures, the way RCP scenarios are set up, and model climate sensitivities all likely contribute to the model spread (Knutti and Hegerl 2008; Szopa et al. 2013; Séférian et al., 2015).

Vertical density profiles help to further explain the changes in stratification. Mean vertical profiles of density in the 1990s and the density change between the 1990s and the 2090s show that all the models become more buoyant at the surface as a consequence of heating and/or freshening of the upper ocean (Figure S1). The density changes at the surface vary by almost a factor of two among models, from -1.1 kg/m^3 (HadGEM) to -0.6 kg/m^3 (GFDL-ES2M), but converge to a relatively narrow range (approximately -0.2 kg/m^3) at 500 m depth. Most of the density change occurs between the surface and 200 m. Below 200 m, the density change in most of the models varies linearly with depth. Thus, our definition of the stratification index, as the density difference between the surface and 200 m, appears reasonable. The converging reductions in density among models at about 500 m agrees with some previous studies based on observations and CMIP3 models (Bindoff et al. 2007; Capotondi et al. 2012; Lyman et al. 2010). Compared to WOA09 data, the models generally underestimate the density of the upper ocean (<150 m) and most models overestimate the density below 350 m (resulting in a positive stratification bias) (Figure S1a).

Vertical profiles of temperature and salinity from each model are also shown in Figure S1. The surface ocean exhibits strong warming of 1.7-3.5°C by the 2090s and the warming magnitude declines quickly with depth, which is associated with the heat uptake capacity of individual models. For instance, GFDL models seem to be more efficient in transporting heat downward than the IPSL models. Above 300 m, the temperature changes vary widely among the models. Temperature changes as a function of depth are complex, and model-to-model differences may be related to a number of factors including rates of vertical mixing and the seasonal thermocline dynamics. At the depth of 500 m, the mean temperature change converges at about 1.2°C. The ocean heat uptake capacity is linked to ocean diapycnal mixing and other processes, such as mixing by mesoscale eddies, which influence the rates of warming in the ocean interior. It is assumed that a model with a weak vertical temperature gradient in the control state has a larger capacity for downward heat transport (Kuhlbrodt and Gregory 2012). The heat uptake capacity of GFDL models could be large as the temperature gradients are weaker than for other models. The large model spread in temperature profiles suggests considerable differences and uncertainties in the parameterizations of these physical processes across the models. Vertical profiles of salinity are more scattered than for temperature (Figure S1c). In the 1990s, most of the models underestimate salinity from the surface down to 550 m. Surface salinity is generally biased low by 0.05-0.25 psu. Most of the freshening with climate change takes place above 100 m, which also acts to increase stratification. Note that the salinity increases at 100-300m in some models (IPSL, GFDL-ESM2M, HadGEM2-ES) partially compensates the impact of rising temperatures on density.

The relative contribution (%) of temperature change to the stratification change from the 1990s to the 2090s is shown in Figure S2. Previous studies have shown that salinity contributes significantly to the stratification changes at high latitudes (>40°) in both hemispheres and in the North Pacific as a consequence of increases in precipitation (e.g., Bindoff et al. 2007). From our comparisons, temperature dominates the stratification changes in the tropical and sub-tropical regions (Figure S2). Salinity dominates the stratification changes in the much of the Arctic Ocean and in the high-latitude North Atlantic. While stratification is a function of SSS and SST to a good approximation (Cabré et al. 2015), stratification change at high latitudes is also dependent on temperature and salinity at depth as vertical mixing and exchange are stronger.

In some regions the spatial distributions and the driving process differs substantially across models. Generally, the models agree well in the tropics and subtropical gyres that surface warming drives increasing stratification. In the high latitude North Atlantic, the subpolar Pacific and the western Pacific Ocean, there is weaker agreement across the models. In the subtropical gyre of the south Pacific, stratification changes in the IPSL and CESM1-BGC models are more dominated by temperature changes, while the other models exhibit more complicated spatial patterns. In the North Atlantic, salinity contributes more in the IPSL and HadGEM2 models than in other models. The southeastern Pacific is more dominated by salinity in the two GFDL models. In the Southern Ocean, the models show relatively large contributions from both salinity and temperature but with complicated spatial patterns that differ substantially across models. Projections for the regions where the models do not agree even on the driving factor should be viewed with more caution. Climate change trends in these regions tend to be projected with less significance across models, for instance, shown in Fig. 1 of Cabré et al. (2015).

The spatial patterns of the changes in stratification are displayed for all the models in Figure 2. Stratification increases globally in all the models with climate change. Nearly all the models predict large increases in stratification in the western tropical Pacific, the tropical Indian Ocean, the Arctic Ocean, and in the high latitude North Atlantic (particularly in the Labrador Sea). The Southern Ocean has weaker increases in stratification, partly because the surface layer mixing and upwelling are intensified due to the poleward shift of strengthened westerly jets (Swart and Fyfe 2012; Sallée et al., 2013; Bracegirdle et al., 2013; Hauck et al., 2015; Leung et al., 2015; Ito et al., 2015). Our stratification index may underestimate the changes in the high latitude North Atlantic, as the relatively deep mixing means that temperature and salinity at 200m depth are changing much more rapidly than in other regions. Reductions in the deep winter mixing and NADW formation in this region are a common pattern seen in strong warming climate simulations (e.g., Cheng et al., 2013; Schwinger et al., 2014). Less drastic increases in stratification are seen over much of the rest of the oceans, with only a few small regions showing decreases in stratification in some models. An exception is the HadGEM2-ES model which has large stratification reductions in the Arctic (Figure 2).

3.2 Surface Nutrient Trends with Climate Change

One of the key factors determining global NPP is nutrient availability in the euphotic zone. Time series of global mean nutrient (0-100m) concentrations for nitrate (NO_3), phosphate (PO_4), silicic acid (SiO_4) and dissolved iron (dFe) are presented in Figure 3. The magnitude of surface nutrient concentrations differs substantially across the models (varying by a factor of ~1.5-2, and by a factor of 5 for dissolved iron). The IPSL models have relatively low surface nutrient concentrations. Compared to the WOA09, 2 models overestimate phosphate (CESM1(BGC) and GFDL-ESM2G) and 5 models overestimate nitrate. All of the models overestimate the silicic acid observations, with the exception of CESM1(BGC). The CESM1(BGC) model overestimates surface phosphate concentrations initially, due to excessive nitrogen limitation, but then shows the strongest surface phosphate declines over the 21st century (Figure 3; Moore et al. 2013).

Over the entire period from 1850-2100, the models all display decreasing trends for surface nitrate, phosphate and silicic acid. Interestingly, surface iron concentrations increase modestly in all but one of the models by 4-10%. Changes in iron concentrations impact marine productivity, nitrogen fixation rates, and oceanic net CO_2 uptake. In the CMIP5 simulations, iron inputs to the oceans were held constant over time, so the increasing surface iron concentrations may reflect increasing macronutrient limitation of phytoplankton growth, leading to reduced biological uptake of iron. The reductions in the sinking export flux also reduce the particle scavenging loss term for dissolved iron. In the CESM1-BGC model, increased production in the High Nutrient, Low Chlorophyll (HNLC) regions offset ~25% of the reduction observed in the macronutrient-limited areas with climate change, while changing circulation patterns also altered the lateral transport of iron within the oceans (Misumi et al. 2014; Moore et al. 2013).

The relative changes in nutrient concentrations (0-100m) (normalized to 1990s means) are presented in Figure 4. The relative changes in the historical run show a consistent pattern across the models for nitrate, phosphate and dissolved iron (except for HadGEM2-ES). In the RCP8.5 projection, the models show diverging estimates of magnitude of the relative changes. For nitrate, the reductions range between -3 to -14% and the phosphate changes range between -3 to -20%. Silicic acid and iron trends are even more variable than for nitrate and phosphate. For silicic acid, there are 3 models showing slight increases, while the others exhibit decreases ranging from ~5-17%. The variability in relative change in silicic acid concentration in the RCP8.5 is likely associated with changes in plankton community and variable diatom production (Bopp et al. 2005). All of the models include some representation of diatoms (Table 2) but the match to observed silicic acid for the current era is generally poor (Figure 3).

The spatial distributions of mean nitrate concentration for 0-100 m in the 1990s are shown in Figure S3. The CMIP5 models reproduce key observed features of the basin scale distributions of surface nitrate. For example, in the eastern equatorial Pacific, Southern Ocean, subarctic North Atlantic and subarctic Pacific exhibit elevated nitrate concentrations in all the models. In the subtropical gyres of the Atlantic and Pacific basins, the mean nitrate concentration is low. However, inter-model comparisons show clear disagreements in some key regions. For example, the details of the high-nitrate water distributions vary considerably in the eastern equatorial Pacific. The HNLC condition extends too far north and south of the equator in some models, and too far to the west in others (Figure S3). The models also differ in the intensity and extent of high nitrate concentration waters in the subarctic North Pacific, where 6 of 9 models show lower nitrate concentrations than the WOA09 data (MPI-ESM-LR, MPI-ESM-MR and HadGEM2-ES are closest to observations). There are also differences in the Arabian Sea and Bay of Bengal, where most models underestimate nitrate concentrations except the GFDL-ESM2M and MPI-ESM-LR models.

Inter-model spread in NPP during the 1990s is pronounced, with NPP as low as 29 PgC yr^{-1} (IPSL-CM5A-LR and IPSL-CM5A-MR), while NPP in one model exceeds 75 PgC yr^{-1} (GFDL-ESM2M) (Table 3, Figure 5). In addition, the spatial pattern of NPP is not well represented by the multi-model mean (Bopp et al. 2013). Satellite based estimation of NPP is approximately 50 PgC yr^{-1} (Behrenfeld et al. 2006; Carr et al. 2006; Anav et al., 2013). The MPI-ES-MR and CESM1-BGC models had NPP of 49.8 PgC yr^{-1} and 54.2 PgC yr^{-1}, closer to the satellite-based estimates, and the observationally constrained model estimate of 56 PgC yr^{-1} by Buitenhuis et al. (2013a). The magnitude of EP also varies substantially across models in the 1990s, ranging from 4.4 to 7.2 PgC yr^{-1} (Table 3).

3.3 Climate Change Impacts on NPP and EP

All of the models exhibit decreasing trends in global NPP and EP with climate change as shown in previous studies (Bopp et al. 2013; Cabré et al., 2015; Laufkötter et al., 2015), and most models show more rapid decreases during the middle to latter part of the 21st century (Figures 5-6, Table 3). All nine models project decreases in export production under RCP8.5 exceeding 5% relative to levels in the 1990s, whereas the response for NPP is divided into 2 groups after 2020. The CESM1(BGC) and GDFL models experience smaller changes in NPP (< 5% relative to 1990s) while other models have larger decreases (8-16%). The largest relative change for NPP is about -16% (MPI-ESM-LR). The EP decreases range from 7% (GFDL-ESM2G) to 28% (IPSL-CM5A-LR). Cabré et al. (2015) showed reductions in NPP and EP for all biomes, except at the highest latitudes. The reductions in global NPP and EP co-vary with the increases in stratification (Figure 6). By the 2090s, stratification increases by about 16% in GFDL-ESM2M and up to 33% in HadGEM1-ES. The rate of stratification increase is slower in the two GFDL models and CESM1(BGC), which also agrees with the slower rates of relative NPP and EP change.

The variability across models in NPP is substantially larger than that seen in EP (Table 3). The normalized standard deviation was +/- 27 % for NPP, but only +/- 12 % for EP in the 1990s. The large spread in simulated NPP and its response to climate change was also noted by Laufkötter et al. (2015a). Seven of the nine models have an EP between 6 and 7.2 PgC yr^{-1} in the 1990s, and the HadGEM2-ES and GFDL-ESM2G models had lower EP (< 5 PgC yr^{-1}). EP is tightly coupled to new nutrient inputs to the euphotic zone in these models. NPP is less tightly coupled as the fraction of regenerated production varies across the models, and can vary spatially and temporally within some models. Thus, the large spread in NPP is not mainly a function of the different physical models and their transport of nutrients to the euphotic zone, but rather it is strongly impacted by the community structure and export efficiency inherent in the models, and the resulting varying levels of regenerated production.

The sinking carbon flux out of the euphotic zone to net primary production ratio (particle export ratio or pe-ratio) is a measure of the export efficiency and also reflects the variable contribution of regenerated production to total NPP (Dugdale and Goering 1967; Eppley and Peterson, 1979; Dunne et al., 2007). High pe-ratio values are typically associated with productive ecosystems dominated by larger phytoplankton (often diatoms, Buesseler, 1998; Boyd and Newton, 1989), while low pe-ratios are associated with oligotrophic food webs with most carbon flow through the microbial loop (Pomeroy, 1974; Azam et al. 1983). The CMIP5 models that include both large and small phytoplankton, assume a higher export efficiency for the large phytoplankton (Moore et al., 2004; 2013; Aumont and Bopp 2006; Séférian et al. 2013; Tjiputra et al. 2013; Laufkötter et al., 2015b).

The fraction of grazed material routed to sinking export is higher, often by a factor of 3-6 than the fraction routed to sinking export for the small phytoplankton (see Laufkötter et al., 2015b for detailed discussion). Diatoms are also likely to dominate phytoplankton blooms in these models. This can drive additional, very efficient, export through aggregation, further enhancing the differences in export efficiency between large and small phytoplankton. Relative to the 1990s, six of the nine models show decreasing trends in the pe-ratio (up to 10% reduction) (Figures 5-6, Table 3; see also Cabré et al., 2015). Diatoms accounted for a smaller percentage of NPP in the 2090s than in the 1990s in all the models, except for the MPI model, where nearly all of the production is by diatoms and the smallest phytoplankton are not explicitly represented (Table 3).

3.4 Increasing Stratification and Declining Nutrients, NPP, and EP

We quantify the relations between stratification and key biogeochemical variables with annual model output over the entire time period of 1850-2100. This approach is more robust than focusing only on the differences between beginning and end of century output (Bopp et al., 2013; Cabré et al., 2015; Laufkötter et al., 2015). Relative changes in global NPP between the 1990s and the 2090s are plotted against the relative change in stratification in Figure 7a. Across all the ESMs, a good relationship is found with a correlation $r^2=0.72$. Larger relative increases in stratification correspond to larger declines in NPP. In addition, the globally-fitted line with a slope of 0.38 separates the models into two groups. In one group (GFDL, IPSL and CESM1-BGC), the NPP reductions are more modest as stratification increases; the other group is composed of the two MPI models, HadGEM1-ES and the NorESM model, which show more intense and linear reductions in NPP with increasing stratification. The reduction of NPP can be partly explained by nutrient changes responding to stratification increases. Across the models, surface nitrate and phosphate concentrations clearly decline as the stratification is enhanced (Figure 7c and 7d, with r^2 of 0.80 and 0.82, respectively). Note that all of these trends are robust across the full time series. Compared to the 1990s, the preindustrial stratification is weaker, surface nutrient concentrations are higher, and NPP and EP are elevated (Figures 3-7). The response of surface silicic acid to increasing stratification is more variable. The projected changes are more divided, as three models (MPI-ESM-LR, MPI-ESM-MR and HadGEM1-ES) show slight increases and the others show reductions in surface silicic acid concentrations (Figure 7b).

EP is even more closely related to the stratification changes (R^2=0.89) than NPP (Figure 7e). The EP change is also closely related to the NPP changes. EP decreases by up to 20% (Figure 7e) whereas NPP decreases by 10-18%. The models display two patterns in terms of the response of NPP and EP to climate change. The first group includes five models (IPSL models, CESM1(BGC) and the GFDL models) where the relative declines in NPP are smaller than the relative declines in EP by a factor of 2 or more (Figure 6 and Table 3). In this group, the EP drops by about 10% and the NPP decreases by 5% or less. In the remaining models the relative declines in EP and NPP are larger and more similar in magnitude. For example, both EP and NPP decrease by about 14% in the HadGEM2-ES model. The differential declines in NPP and EP in the first group of models documents declining export efficiency for the ocean biological pump, driven by phytoplankton community shifts and a decreased contribution to NPP by large phytoplankton (diatoms) (see below and Figures 6-10; also Cabré et al., 2015).

Reduced nutrient availability seems to be a major contributor to declines in NPP and EP. However, the relationship varies from one model to another because growth and export are complicated functions of macronutrient limitation, temperature, irradiance and iron limitation, as well as the routing of organic matter within the ecosystem that drives export efficiency. Higher metabolic rates with warming can be compensated to a large degree by changes in the supply of nutrients and altered light in terms of globally integrated productivity (Dutkiewicz et al. 2013). The NPP response is also strongly impacted by phytoplankton community structure, which modifies export efficiency, and the corresponding magnitude of the regenerated primary production. For the IPSL, CESM1(BGC), and GFDL models that show larger declines in EP than in NPP, this pattern is driven by a decreasing contribution to total NPP by large phytoplankton (Table 3, Figures 8-9). Most of the primary production in these models is by smaller phytoplankton. The GFDL models express this pattern most strongly, with minimal declines in NPP, despite declines in EP approaching 10% (Figure 6 and Table 3). The other models tend to have production that is dominated by diatoms, and do not capture the community shifts towards increasing small phytoplankton dominance (and reduced export efficiency) under increasing nutrient stress. The declines in NPP with increasing stratification are more linear and more similar in magnitude to the declines in EP (Figure 7, panels a, b, and h). Thus, there are also very strong correlations between the climate-driven changes in the fractional contribution of diatoms to NPP and both the changes in stratification and the changes in EP (Figure 7, panels f and g, correlations of r^2=0.85 and r^2=0.95, both much higher than the correlation between changing stratification and NPP, r^2=0.71). Cabré et al. (2015) found similar patterns relating community composition, NPP, and EP comparing the period from 1980-1999 with 2080-2099, across low to mid-latitude biomes.

Some of these patterns are illustrated in Figure 8, which shows the contribution of diatoms (large phytoplankton) to NPP for the 1990s. Most of the models show elevated diatom production at high latitudes and lower diatom contributions in the subtropical gyres. However, there are large discrepancies in the magnitude of the diatom contribution, ranging from about 30% to more than 90% in the Arctic Ocean, for example. At the global-scale diatoms account for only 9.4% of NPP in the GFDL-ESM2M model and reach a maximum of 91% in the MPI-ESM-MR model (Table 3). The large variability across the models reflects, in part, the lack of an observational dataset to constrain phytoplankton community composition, at the time these models were being developed. The new globally-gridded ocean atlas of plankton functional types, MAREDAT (Buitenhuis et al. 2013) has started to fill this gap, and should lead to improved representations of plankton community structure in the future as the dataset becomes increasingly populated and is entrained into model development and validation. Remote sensing estimates of phytoplankton community composition and size class structures are also providing useful constraints for global-scale modeling efforts (e.g., Alvain et al., 2005; Hirata et al., 2008; Kostadinov et al., 2009; Siegel et al., 2014).

The spatial patterns of the shifts in phytoplankton community composition with climate change are illustrated in Figure 9, where we plot the change in the percentage of NPP by diatoms (2090s – 1990s). There are some robust trends across the models. One of the areas with the biggest declines in diatom production is the high-latitude North Atlantic. This region typically has some of the biggest stratification increases with climate change, greatly reducing the deep winter mixing that entrains nutrients to the surface (Moore et al. 2013; Cheng et al., 2013; Randerson et al. 2015). Nearly all the models also show large declines in diatom contributions to production in the Arctic Ocean. The CMIP5 models show consistent trends of increasing stratification, declining surface nutrient concentrations, and a longer growing season with climate change in the Arctic (Vancoppenolle et al. 2013). Increasing surface temperatures and dramatic declines in the sea ice cover allow for a longer growing season with climate change. Thus, nutrients in surface waters are more completely used up by summer’s end, leading to community shifts with decreased diatom production and an increased fraction of production by smaller phytoplankton. In the CESM-BGC model, this community shift allows for a small increase in central Arctic NPP, even as export production and surface nutrient concentrations decline, due to the increased fraction of NPP by small phytoplankton and the resulting increases in regenerated production (Moore et al., 2013).

All of the models show some increase in the fraction of NPP by diatoms in the Southern Ocean (Figure 9). The increase is particularly strong in the CESM1-BGC, IPSL, and GFDL models. Most of the models also show some increased diatom production in the tropical Pacific. Bopp et al. (2005) also found decreasing diatom production in the Arctic and high-latitude North Atlantic, with some increases in the Southern Ocean under a strong warming climate scenario. Steinacher et al. (2010) also found declining productivity in the North Atlantic, and shifts in the export ratio due to phytoplankton community shifts with decreasing diatom production. The earlier version of the CESM used in that study (CCSM3) showed only small shifts in export ratios with climate change, as the range in export ratios and the differences in export efficiencies between large and small phytoplankton were smaller than in the CESM (Moore et al. 2013; Steinacher et al. 2010). Three models in this study (HadGEM2-ES and the MPI models) show increased diatom production in the low latitudes (Figure 9).

However, the diatoms dominate production nearly everywhere in these three models (Figure 8).

There are also large inter-model differences in the spatial patterns of the pe-ratio (Figure 10). Some of the models (GFDL, IPSL, CESM-BGC) show a close correlation between the pe-ratio and diatom production (compare Figures 8 and 10), due to the enhanced export efficiency for diatoms (large phytoplankton) built into the models. Thus, there is a very high correlation between the changing contribution of diatoms to NPP and the changes in EP (Figure 7, panel g, Table 3). The MPI model includes one phytoplankton group and has an essentially constant pe-ratio of 0.15, explaining the linearity of the changes in NPP and EP with warming (Figures 8 and 10). Production in the HadGEM1-ES model is dominated nearly everywhere by the diatoms (Figure 8). Therefore, the MPI and HadGEM models cannot capture a shift towards increasing small phytoplankton dominance under declining surface nutrient concentrations. This leads to export production being closely correlated with diatom production in these models as most production is by diatoms, as well as in the other models where diatoms are assumed to export more efficiently but account for a smaller fraction of total NPP (Table 3).

There is also a strong correlation between the declines in the fraction of NPP by diatoms and declines in the pe-ratio (compare Figures 7, 9 and 11). The largest declines in the pe-ratio are seen in the Arctic and the high-latitude North Atlantic, regions where diatom production also decreased. The GFDL, IPSL, and CESM1(BGC) models also show some reductions in pe-ratio in the subarctic North Pacific, but the spatial patterns are inconsistent (Figure 11). The models display considerable variability in the degree of stratification increase and in the dominant factor driving these changes in the subarctic North Pacific (Figures S2 and 2).

The correlation for the relationship between the changing percentage of NPP by diatoms versus the changes in EP across all the models has an r^2 value of 0.96 and a slope with a value close to 1 (0.94, Figure 7g) indicating that phytoplankton community structure plays a dominant role in determining the responses of NPP, EP, and the pe-ratio to climate change. The biggest declines in the fraction of production by diatoms and pe-ratios are in precisely the areas where some of the largest increases in upper ocean stratification are seen, along with declining surface nutrient concentrations, as in the Arctic Ocean and in the high latitude North Atlantic (Figures 6-8; see also Moore et al., 2013; Steinacher et al., 2010; Cabré et al., 2015).

3.5 Projected Changes in NPP, EP and Stratification Biases

At global scale, the CMIP5 models show considerable stratification biases for the 1990s when compared to the WOA09 data (Figure 1, Table 3). Only the GFDL-ESM2M model is within 10% of the observed value. From the density profiles as well (Figure S1) it is apparent that most of the models have stronger stratification in the 1990s than seen in the observations. Liu et al. (2014) argued that climate bias is important when projecting the impact of climate change on land surface processes and Hoffman et al. (2014) documented this for atmospheric CO_2 mole fractions. Here, we examine how stratification biases in the 1990s may affect model projections of NPP and EP in the 2090s.

Models with stronger bias in the 1990s for surface stratification tend to predict larger climate-induced declines in both NPP and EP (Figure 12, r^2=0.47 and r^2=0.54, respectively). The slopes are plotted when the correlation is significant at >95% level. Five of the models have positive biases in stratification for the current era that exceed 20%. These models also show the largest relative increases in stratification with climate change of 26-30% (Figure 12, Table 3). The remaining four models (GFDL models, CESM1-BGC, and NorESM1-ME) do a better job of simulating observed stratification for the current era, and predict relative increases in stratification over the 21st century that are roughly half as large, ranging from ~15-18%. This suggests that the more biased models (for the 1990s) may be overestimating the projected reductions in NPP and EP for the end of the century.

4 Discussion and Conclusions

The ESMs analyzed here have different resolutions and incorporate marine biogeochemical-ecosystem models with different mechanisms and degrees of complexity. We find this set of models has consistent trends of increasing stratification and decreasing NPP and EP. However, a large model spread is apparent for the 1990s, particularly for NPP, and in the relative changes to NPP and EP over the 21st century due to climate change. NPP is reduced by 2-18% in the 2090s and EP is reduced by 7-20%. Mean stratification increased by 16% (GFDL-ESM2M) to 33% (HadGEM1-ES) from the 1990s to the 2090s. Under strong warming scenarios like RCP8.5, ocean stratification will continue to rapidly increase after the year 2100 in all of these models (Randerson et al., 2015).

The strongly linear relationship between stratification increases and EP decreases seen within each model and across all the models (Figures 7 and 12) indicates a strong bottom up control on EP, through declining upward nutrient flux to the euphotic zone. Declining surface nutrient concentrations are seen in all the models with climate change under the RCP 8.5 scenario (Figures 5-6). Nitrate is reduced by 3 to 14% and phosphate is reduced by 3 to 20%. Changes in surface silicic acid and iron concentrations are more variable across the models. For silicic acid, there are 3 models showing slight increases, while the others exhibit decreases of 5-17%. With respect to iron, 8 models indicate an increase of 4-10% relative to the 1990s; with the exception being the NorESM-ME model, which is reduced by 3%. Changes in the temperature and light fields also have impacts on EP in some regions, but increasing stratification and nutrient stress, and the resulting impacts on phytoplankton community composition and EP is the dominate process at the global scale. On a global scale, over the full 1850-2100 time period, the changes in NPP and EP are more highly correlated with the changes in stratification, than with the changes in SST (r^2 0.72 for stratification-NPP and 0.66 for SST-NPP, Figure 7). This is because that the stratification metric captures both the temperature-driven changes that dominate at low to mid-latitudes, and the salinity-driven changes at higher latitudes. The relationship between the change of light levels and NPP was shown to be significant only in the sea-ice covered area of south hemisphere by Cabré et al. (2015). The temperature-driven increases in growth rates are offset by reduced nutrient supply in many regions as stratification is increased (Bopp et al. 2005; Cabré et al. 2015).

Simulated NPP and its response to climate change are both more variable across the models than EP, and are less strongly correlated with changes in stratification (Figure 7). This is driven by model differences in the export efficiency of the biological pump and its relation to phytoplankton community structure. The models that allow for shifts in phytoplankton community structure whereby increasing nutrient stress gives competitive advantage to smaller cells over larger cells, show strongly non-linear NPP response to climate change. NPP declines less rapidly than EP with increasing nutrient stress, as the percentage of NPP by large cells declines and export efficiency decreases (and the regenerated production fraction increases). Models without this dynamic community composition and export efficiency show a much more linear NPP response to climate change (Figure 7). Thus, projections of the response of NPP to climate change in the CMIP5 models are critically dependent on the simulated phytoplankton community structure, the efficiency of the biological pump, and the resulting (highly variable) levels of regenerated production.

Spatial patterns of diatom productivity are influenced by changes in surface nutrients and the resulting shifts in plankton community composition. The response of the %NPP by diatoms depends on several factors, including whether they were a small or large component of the community initially. Therefore, the spatial patterns of changes in stratification and %NPP by diatoms can differ (Figure 2 and Figure 9). In the paper, the largest decreases are seen in areas with high diatom production initially and large increases in stratification, particularly in the Northern Hemisphere, leading to North-South hemispheric asymmetry (Marinov et al., 2013; Cabré et al., 2015). In the Southern Ocean, the winds that drive upwelling, strengthen and shift poleward with climate change, influencing iron supply and productivity patterns (Sallée et al., 2013; Leung et al., 2015).

The large spread in the simulated NPP rates for the 1990s and the variability seen across models in the response of NPP to climate change introduce challenges for climate impact and risk assessment, as NPP is a key product of both terrestrial and marine ecosystem models, and changes to NPP are perhaps the most cited result from this class of models. We have demonstrated that the wide spread seen in simulated NPP is not due to the different physical circulation models and the flux of nutrients they deliver to surface waters, but rather to the efficiency of the biological pump (tied to community structure in most models) and the resulting levels of regenerated primary production (see also Cabré et al., 2015). Changes in EP are an additional useful metric of climate impacts on marine ecosystems. EP is more strongly tied to climate feedback, as it is mainly the fixed carbon sequestered to the deeper ocean by the biological pump that will impact air-sea CO_2 exchange. In addition, in terms of impacts up the food chain, EP may be a better metric than NPP. Friedland et al. (2012) demonstrated that there is no correlation between fishery yield and NPP at the global scale, but that there are strong correlations between fishery yield and several other variables including chlorophyll concentration, the pe-ratio, and EP. These three proxies all correlate with the fraction of primary production by large phytoplankton. In this context, the results presented here suggest large future declines in fishery yield across the high-latitude North Atlantic.

Laufkötter et al. (2015a) suggest a strong impact of temperature modification of phytoplankton growth rates and other ecosystem processes (including zooplankton growth and grazing rates) to infer a strong top-down grazing influence on the NPP response to climate change, noting that phytoplankton community growth rates appear to increase at low latitudes in some models, even as available nutrient concentrations decline. Several factors make it difficult to interpret their results and compare to our findings. Many of the key fluxes and fields needed to support their hypotheses were not available in the archived output from the CMIP5 models. They were forced to rely on estimated nutrient limitation factors and growth rates for the only the surface ocean in their analysis. Temperature warming is strongest at the surface (Figure 1S). Thus, their analysis may overestimate the temperature effects for the whole euphotic zone. They also present results based on diatom-specific nutrient limitation patterns, on the phytoplankton group with the largest changes in limitation factors, and on comparing total grazing with total NPP for some models (Figures 6-8, Laufkötter et al. 2015a). This may not be representative of the growth and/or community responses. At low latitudes the diatoms might show the biggest declines in growth due to nutrient limitation, but they may be only a small component of the community in many of the models (Figure 8). Under increasing nutrient stress, phytoplankton community growth rates may increase simply due to a declining contribution from diatoms, as the smaller phytoplankton will typically grow faster at low nutrient concentrations. Looking at total grazing rates compared to NPP cannot account for these community effects. We agree that temperature effects may be important in the NPP climate change response and that the temperature influence on phytoplankton growth and on the ecosystem processing of NPP that leads to export are highly uncertain (Laufkötter et al. 2015a). Sherman et al. (2016) compiled in situ estimates of phytoplankton community growth rates at the global-scale, and found a relatively weak apparent temperature effect (apparent Q_{10} ~ 1.5). The observational estimates of phytoplankton community growth rates were compared with the CESM and GFDL simulations analyzed here. ESMs used in climate change studies need to ensure that the emergent, apparent temperature-growth relation matches this observed value (even though higher explicit Q10 values may be prescribed for individual plankton functional types) to avoid biases in the response to temperature change (Sherman et al., 2016).

Many of the CMIP5 models have an assumed higher export efficiency for diatoms relative to small phytoplankton (Laufkötter et al., 2015b), building on a long-standing paradigm, strengthened by results from the detailed ecosystem studies of the Joint Global Flux Study (JGOFS) program (Boyd and Newton 1999; Buesseler 1998). In the current models, the spectrum of phytoplankton size structure is often represented very simply with only the end members of one large and one small phytoplankton group. Thus, the "diatom" group is a proxy for larger, efficiently-exporting, blooming phytoplankton functional types. DOM cycling, heterotrophic bacteria, microzooplankton, and the microbial loop are typically treated in an idealized, implicit manner in the current models as well.

To accurately predict the response of NPP and EP to climate change, it may be necessary to develop more robust ecosystem models with additional explicit phytoplankton, heterotrophic microbial, and zooplankton groups, including their impacts on nutrient cycling, export efficiency and the downward transport of organic matter. Models that include much greater diversity in the phytoplankton, show large community composition shifts with climate change (Dutkiewicz et al. 2013). Quantifying the links between NPP, EP and community composition in observational datasets are a high priority. There are only limited field observations of the pe-ratio, some of which rely on nutrient drawdown and other indirect estimates of the sinking particle flux (Dunne et al. 2007). Further progress to improve model performance requires combined efforts from satellite, field, and laboratory observations, empirical and inverse modeling approaches, as well as process-based, forward models.

The large model spread in EP and NPP, and significant biases seen in key nutrient fields for the 1990s suggest that the current ocean biogeochemical models are far from perfect and their results must be interpreted with some caution. However, the relationships between stratification and EP, NPP and nutrients do reveal some common mechanisms driving the climate change response. The large inter-model differences for the current era in NPP, EP and nutrient concentrations are partially associated with how these biogeochemical models are initialized and spun up for these experiments. The ocean biogeochemical models are often integrated in an offline mode for a thousand years or more before coupling to other components of the ESM (Séférian et al., 2016). The achieved preindustrial, near-steady state of biogeochemical fields may deviate substantially from the observed climatology, driven by biases in the physics and biogeochemistry. These differences typically persist in the present-day simulations and future projections. The advantage of the initialization and spin up process is that the biogeochemical fields are consistent with the simulated ocean circulation, and will respond to climate-driven changes appropriately. The strong intrinsic variability helps to reduce model drift and generate reasonable longer-term variability. As a result, these long-term simulations are suitable for analyzing climate trends, variability and sensitivities. RCP 8.5 is a strong warming scenario and the relationship between stratification changes and NPP/EP changes may be somewhat different under other RCP scenarios. Although the relations between the degree of surface warming and the ocean biogeochemical responses were largely linear across RCP 4.5 and 8.5 for the CESM(BGC) (Moore et al. 2013).

Some potentially important marine biogeochemical feedbacks on the climate system were missing completely or not well represented in the CMIP5 models, including important feedbacks through aerosol transport and deposition on the marine iron cycle, feedbacks involving the oxygen minimum zones and the marine nitrogen cycle, and the impacts on ocean biology by ongoing ocean acidification. Each of these feedbacks could impact phytoplankton and zooplankton community structures, NPP, EP, and pe-ratios in the future.

It is also important to consider the longer-term climate change responses of both ocean physics and marine biogeochemistry. Moore et al. (2013) noted that climate impacts on the oceans were still accelerating at year 2100 under the RCP

8.5 scenario (but not under the more moderate RCP 4.5 scenario). Randerson et al. (2015) extended the CESM1(BGC) RCP 8.5 scenario simulation examined here, to the year 2300. In these longer simulations, the climate impacts on ocean physical fields and biogeochemistry lead to even stronger perturbations after 2100 than those presented here for the 2090s. In addition, the ocean contribution to the climate-carbon feedback exceeded the land contribution after the year 2100 (Randerson et al. 2015).

5 Acknowledgments

We are grateful for support from the U.S. Dept. of Energy Office of Science and the National Science Foundation (NSF). This contribution was supported by a grant to UCI as a part of the BGC Feedbacks Scientific Focus Area within the Regional and Global Climate Modeling (RGCM) Program in the Climate and Environmental Sciences Division (CESD) of the Biological and Environmental Research (BER) Program in the US Dept. of Energy Office of Science. We also received funding from the NSF project "Collaborative Research: Improved Regional and Decadal Predictions of the Carbon Cycle"(AGS-1048890). We would also like to thank all those in the CMIP5 project efforts, which made this work possible.

6 References

Uncategorized References

Alvain, S.; Moulin, C.; Dandonneau, Y.; Breon, F.M., 2005: Remote sensing of phytoplankton groups in case 1 waters from global SeaWiFS imagery. *Deep Sea Res. Part I*, *1*, 1989–2004.

Aumont, O., and L. Bopp, 2006: Globalizing results from ocean in situ iron fertilization studies. *Global Biogeochemical Cycles*, **20**.

Azam, F., T. Fenchel, J. G. Field, J. S. Gray, L. A. Meyerreil, and F. Thingstad, 1983: The Ecological Role Of Water-Column Microbes In The Sea. *Marine Ecology Progress Series*, **10,** 257-263.

Behrenfeld, M. J., and Coauthors, 2006: Climate-driven trends in contemporary ocean productivity. *Nature*, **444,** 752-755.

Bentsen, M., and Coauthors, 2013: The Norwegian Earth System Model, NorESM1-M - Part 1: Description and basic evaluation of the physical climate. *Geoscientific Model Development*, **6,** 687-720.

Bindoff, N. L., and Coauthors, 2007: Observations: oceanic climate change and sea level. Cambridge University Press, 385-432.

Bopp, L., O. Aumont, P. Cadule, S. Alvain, and M. Gehlen, 2005: Response of diatoms distribution to global warming and potential implications: A global model study. *Geophysical Research Letters*, **32**.

Bopp, L., and Coauthors, 2001: Potential impact of climate change on marine export production. *Global Biogeochemical Cycles*, **15,** 81-99.

Bopp, L., and Coauthors, 2013: Multiple stressors of ocean ecosystems in the 21st century: projections with CMIP5 models. *Biogeosciences*, **10,** 6225-6245.

Boyd, P. W., and P. P. Newton, 1999: Does planktonic community structure determine downward particulate organic carbon flux in different oceanic provinces? *Deep-Sea Research Part I-Oceanographic Research Papers*, **46,** 63-91.

Bracegirdle, T. J., E. Shuckburgh, J.-B. Sallee, Z. Wang, A. J. S. Meijers, N. Bruneau, T. Phillips, and L. J. Wilcox, 2013: Assessment of surface winds over the Atlantic, Indian, and Pacific Ocean sectors of the SouthernOcean in CMIP5models: historical bias, forcing response, and state dependence, J. Geophys. Res. Atmos., 118, 547–562, doi:10.1002/jgrd.50153.

Buesseler, K. O., 1998: The decoupling of production and particulate export in the surface ocean. *Global Biogeochemical Cycles*, **12,** 297-310.

Buitenhuis, E. T., T. Hashioka, and C. L. Quere, 2013a: Combined constraints on global ocean primary production using observations and models, Global Biogeochem. Cycles, 27, 847–858, doi:10.1002/gbc.20074.

Buitenhuis, E., and Coauthors, 2013b: MAREDAT: towards a world atlas of MARine Ecosystem DATa. *Earth System Science Data*, **5,** 227-239.

Cabré, A., I. Marinov, and S. Leung, 2015: Consistent global responses of marine ecosystems to future climate change across the IPCC AR5 earth system models. *Climate Dynamics*, **45,** 1253-1280.

Capotondi, A., M. A. Alexander, N. A. Bond, E. N. Curchitser, and J. D. Scott, 2012: Enhanced upper ocean stratification with climate change in the CMIP3 models. *Journal of Geophysical Research-Oceans*, **117**.

Carr, M.-E., and Coauthors, 2006: A comparison of global estimates of marine primary production from ocean color. *Deep-Sea Research Part Ii-Topical Studies in Oceanography*, **53,** 741-770.

Cheng, W., Chiang, J.C.H., and D. Zhang, 2013: Atlantic meridional overturning circulation (AMOC) in CMIP5 model: RCP and Historical simulations. J. Climate, 26: 7187-7197, doi: 10.1175/JCLI-D-12-00496.

Collins, W. J., and Coauthors, 2011: Development and evaluation of an Earth-System model-HadGEM2. *Geoscientific Model Development*, **4,** 1051-1075.

Dufresne, J. L., and Coauthors, 2013: Climate change projections using the IPSL-CM5 Earth System Model: from CMIP3 to CMIP5. *Climate Dynamics*, **40,** 2123-2165.

Dugdale, R. C., and J. J. Goering, 1967: Uptake of new and regenerated forms of nitrogen in primary productivity. *Limnology and Oceanography*, **12,** 196-206.

Dunne, J. P., J. L. Sarmiento, and A. Gnanadesikan, 2007: A synthesis of global particle export from the surface ocean and cycling through the ocean interior and on the seafloor. *Global Biogeochemical Cycles*, **21**.

Dunne, J. P., and Coauthors, 2013: GFDL's ESM2 Global Coupled Climate-Carbon Earth System Models. Part II: Carbon System Formulation and Baseline Simulation Characteristics. *J Climate*, **26,** 2247-2267.

Dunne, J. P., and Coauthors, 2012: GFDL's ESM2 Global Coupled Climate-Carbon Earth System Models. Part I: Physical Formulation and Baseline Simulation Characteristics. *J Climate*, **25,** 6646-6665.

Dutkiewicz, S., J. R. Scott, and M. J. Follows, 2013: Winners and losers: Ecological and biogeochemical changes in a warming ocean. *Global Biogeochemical Cycles*, **27,** 463-477.

Eppley, R. W., and B. J. Peterson, 1979: Particulate Organic-Matter Flux And Planktonic New Production In The Deep Ocean. *Nature*, **282,** 677-680.

Friedland, K. D., and Coauthors, 2012: Pathways between primary production and fisheries yields of large marine ecosystems. *PLoS One*, **7,** e28945.

Froelicher, T. L., F. Joos, G. K. Plattner, M. Steinacher, and S. C. Doney, 2009: Natural variability and anthropogenic trends in oceanic oxygen in a coupled carbon cycle-climate model ensemble. *Global Biogeochemical Cycles*, **23**.

Fung, I. Y., S. C. Doney, K. Lindsay, and J. John, 2005: Evolution of carbon sinks in a changing climate. *Proceedings of the National Academy of Sciences of the United States of America*, **102,** 11201-11206.

Garcia, H. E., R. A. Locarnini, M. M. Zweng, O. K. Baranova, and D. R. Johnson, 2010. Nutrients (Phosphate, Nitrate, Silicate). Vol. 4, World Ocean Atlas 2009, NOAA Atlas NESDIS 71,398 pp.

Gent, P. R., and Coauthors, 2011: The Community Climate System Model Version 4. *J Climate*, **24,** 4973-4991.

Giorgetta, M. A., and Coauthors, 2013: Climate and carbon cycle changes from 1850 to 2100 in MPI‐ESM simulations for the Coupled Model Intercomparison Project phase 5. *Journal of Advances in Modeling Earth Systems*, **5,** 572-597.

Goldstein, B., F. Joos, and T. F. Stocker, 2003: A modeling study of oceanic nitrous oxide during the Younger Dryas cold period. *Geophysical Research Letters*, **30**.

Bracegirdle, T. J., E. Shuckburgh, J.-B. Sallee, Z. Wang, A. J. S. Meijers, N. Bruneau, T. Phillips, and L. J. Wilcox, 2013: Assessment of surface winds over the Atlantic, Indian, and Pacific Ocean sectors of the SouthernOcean in CMIP5models: historical bias, forcing response, and state dependence, J. Geophys. Res. Atmos., 118, 547–562, doi:10.1002/jgrd.50153.

Hannon, E., P. W. Boyd, M. Silvoso, and C. Lancelot, 2001: Modeling the bloom evolution and carbon flows during SOIREE: Implications for future in situ iron-enrichments in the Southern Ocean. *Deep-Sea Research Part Ii-Topical Studies in Oceanography*, **48,** 2745-2773.

Hauck, J., et al. (2015), On the Southern Ocean CO2 uptake and the role of the biological carbon pump in the 21st century, *Global Biogeochem. Cycles*, *29*, 1451–1470, doi:10.1002/2015GB005140

Hirata, T.; Hardman-Mountford, N.J.; Brewin, R.J.W.; Aiken, J.; Barlow, R.; Suzuki, K.; Isada, T.; Howell, E.; Hashioka, T.; Aita-Noguchi, M.; *et al.*, 2008: Synoptic relationships between surface Chlorophyll-a and diagnostic pigments specific to phytoplankton functional types. *Biogeosciences*, *8*, 311–327.

Ilyina, T., K. D. Six, J. Segschneider, E. Maier‐Reimer, H. Li, and I. Núñez‐Riboni, 2013: Global ocean biogeochemistry model HAMOCC: Model architecture and performance as component of the MPI‐Earth system model in different CMIP5 experimental realizations. *Journal of Advances in Modeling Earth Systems*, **5,** 287-315.

Ito, T., A. Bracco, C. Deutsch, H. Frenzel, M. Long, and Y. Takano (2015), Sustained growth of the Southern Ocean carbon storage in a warming climate, Geophys. Res. Lett., 42, 4516–4522, doi:10.1002/2015GL064320.

Kostadinov, T.S.; Siegel, D.A.; Maritorena, S., 2009: Retrieval of the particle size distribution from satellite ocean color observations. *J. Geophys. Res.*, *114*, C09015.

Jin, X., N. Gruber, J. P. Dunne, J. L. Sarmiento, and R. A. Armstrong, 2006: Diagnosing the contribution of phytoplankton functional groups to the production and export of particulate organic carbon, CaCO3, and opal from global nutrient and alkalinity distributions. *Global Biogeochemical Cycles*, **20**.

Jones, C., and Coauthors, 2011: The HadGEM2-ES implementation of CMIP5 centennial simulations. *Geoscientific Model Development*, **4,** 543-570.

Knutti, R., and G. C. Hegerl, 2008: The equilibrium sensitivity of the Earth's temperature to radiation changes. *Nature Geoscience*, **1,** 735-743.

Kuhlbrodt, T., and J. M. Gregory, 2012: Ocean heat uptake and its consequences for the magnitude of sea level rise and climate change. *Geophysical Research Letters*, **39**.

Laufkötter, C., Vogt, M., Gruber, N., Aumont, O., Bopp, L., Doney, S. C., Dunne, J. P., Hauck, J., John, J. G., Lima, I. D., Seferian, R., and Völker, C., 2015: Projected decreases in future marine export production: the role of the carbon flux through the upper ocean ecosystem, Biogeosciences Discuss., 12, 19941-19998, doi:10.5194/bgd-12-19941-2015.

Laufkötter, C., Vogt, M., Gruber, N., Aita-Noguchi, M., Aumont, O., Bopp, L., Buitenhuis, E., Doney, S. C., Dunne, J., Hashioka, T., Hauck, J., Hirata, T., John, J., Le Quéré, C., Lima, I. D., Nakano, H., Seferian, R., Totterdell, I., Vichi, M., and Völker, C., 2015: Drivers and uncertainties of future global marine primary production in marine ecosystem models, Biogeosciences, 12, 6955-6984, doi:10.5194/bg-12-6955-2015.

Le Quere, C., and Coauthors, 2005: Ecosystem dynamics based on plankton functional types for global ocean biogeochemistry models. *Global Change Biology*, **11,** 2016-2040.

Leung, S., Cabré, A., and I. Marinov, 2015: A latitudinally banded phytoplankton response to 21st century climate change in the Southern Ocean across the CMIP5 model suite. Biogeosciences, 12, 5715–5734, doi:10.5194/bg-12-5715-2015.

Liu, M., and Coauthors, 2014: What is the importance of climate model bias when projecting the impacts of climate change on land surface processes? *Biogeosciences*, **11,** 2601-2622.

Luo, Y. Y., Q. Y. Liu, and L. M. Rothstein, 2009: Simulated response of North Pacific Mode Waters to global warming. *Geophysical Research Letters*, **36**.

Lyman, J. M., and Coauthors, 2010: Robust warming of the global upper ocean. *Nature*, **465,** 334-337.

Manizza, M., C. Le Quere, A. J. Watson, and E. T. Buitenhuis, 2008: Ocean biogeochemical response to phytoplankton-light feedback in a global model. *Journal of Geophysical Research-Oceans*, **113**.

Marinov, I., S. C. Doney, I. D. Lima, K. Lindsay, J. K. Moore, and N. Mahowald, 2013: North-South asymmetry in the modeled phytoplankton community response to climate change over the 21st century. *Global Biogeochemical Cycles*, **27,** 1274-1290.

Misumi, K., K. Lindsay, J. Moore, S. Doney, F. Bryan, D. Tsumune, and Y. Yoshida, 2014: The iron budget in ocean surface waters in the 20th and 21st centuries: projections by the Community Earth System Model version 1. *Biogeosciences*, **11,** 33-55.

Moore, J., K. Lindsay, S. Doney, M. Long, and K. Misumi, 2013: Marine Ecosystem Dynamics and Biogeochemical Cycling in the Community Earth System Model [CESM1(BGC)]: Comparison of the 1990s with the 2090s under the RCP4.5 and RCP8.5 Scenarios. *J Climate*, **26,** 9291-9312.

Moore, J. K., S. C. Doney, and K. Lindsay, 2004: Upper ocean ecosystem dynamics and iron cycling in a global three-dimensional model. *Global Biogeochemical Cycles*, **18,** n/a-n/a.

Moss, R. H., and Coauthors, 2010: The next generation of scenarios for climate change research and assessment. *Nature*, **463,** 747-756.

Pahlow, M., and U. Riebesell, 2000: Temporal trends in deep ocean Redfield ratios. *Science*, **287,** 831-833.

Passow, U., and C. A. Carlson, 2012: The biological pump in a high CO2 world. *Marine Ecology Progress Series*, **470,** 249-271.

Plattner, G. K., F. Joos, T. F. Stocker, and O. Marchal, 2001: Feedback mechanisms and sensitivities of ocean carbon uptake under global warming. *Tellus Series B-Chemical and Physical Meteorology*, **53,** 564-592.

Pollard, R. T., and Coauthors, 2009: Southern Ocean deep-water carbon export enhanced by natural iron fertilization. *Nature*, **457,** 577-U581.

Pomeroy, L. R., 1974: The ocean's food web, a changing paradigm. *Bioscience*, **24,** 499-504.

Randerson, J. T., K. Lindsay, E. Munoz, W. Fu, J. K. Moore, F. M. Hoffman, N. M. Mahowald, and S. C. Doney (2015), Multicentury changes in ocean and land contributions to the climate-carbon feedback, Global Biogeochem. Cycles, 29,doi:10.1002/2014GB005079.

Sallée, J.-B., E. Shuckburgh, N. Bruneau, A. J. S. Meijers, T. J. Bracegirdle, Z. Wang, and T. Roy, 2013: Assessment of Southern Ocean water mass circulation and characteristics in CMIP5 models: Historical bias and forcing response, *J. Geophys. Res. Oceans*, *118*, 1830–1844, doi:10.1002/jgrc.20135.

Schmittner, A., and E. D. Galbraith, 2008: Glacial greenhouse-gas fluctuations controlled by ocean circulation changes. *Nature*, **456,** 373-376.

Schmittner, A., A. Oschlies, H. D. Matthews, and E. D. Galbraith, 2008: Future changes in climate, ocean circulation, ecosystems, and biogeochemical cycling simulated for a business-as-usual CO2 emission scenario until year 4000 AD. *Global Biogeochemical Cycles*, **22**.

Séférian, R., and Coauthors, 2013: Skill assessment of three earth system models with common marine biogeochemistry. *Climate Dynamics*, **40,** 2549-2573.

Séférian, R., M. Gehlen, L. Bopp, L. Resplandy, J. C. Orr2, O. Marti, J. P. Dunne, J. R. Christian, S. C. Doney, T. Ilyina, K. Lindsay, P. Halloran, C. Heinze, J. Segschneider, and J. Tjiputra, 2015: Inconsistent strategies to spin up models in CMIP5: implications for ocean biogeochemical model performance assessment. Geosci. Model Dev. Discuss., 8, 8751–8808. doi:10.5194/gmdd-8-8751-2015.

Sherman, E., J. K. Moore, F. Primeau, and D. Tanouye, 2016: Temperature influence on phytoplankton community growth rates, Global Biogeochem. Cycles, 30, doi:10.1002/2015GB005272.

Siegel, D. A., K. O. Buesseler, S. C. Doney, S. F. Sailley, M. J. Behrenfeld, and P. W. Boyd, 2014: Global assessment of ocean carbon export by combining satellite observations and food-web models, Global Biogeochem. Cycles, 28, doi:10.1002/2013GB004743.

Siegenthaler, U., and T. Wenk, 1984: Rapid Atmospheric Co2 Variations And Ocean Circulation. *Nature*, **308,** 624-626.

Steinacher, M., F. Joos, T. L. Froelicher, G. K. Plattner, and S. C. Doney, 2009: Imminent ocean acidification in the Arctic projected with the NCAR global coupled carbon cycle-climate model. *Biogeosciences*, **6,** 515-533.

Steinacher, M., and Coauthors, 2010: Projected 21st century decrease in marine productivity: a multi-model analysis. *Biogeosciences*, **7,** 979-1005.

Swart, N. C., and J. C. Fyfe, 2012: Observed and simulated changes in the Southern Hemisphere surface westerly wind-stress. *Geophysical Research Letters*, **39**.

Szopa, S., and Coauthors, 2013: Aerosol and ozone changes as forcing for climate evolution between 1850 and 2100. *Climate Dynamics*, **40,** 2223-2250.

Taylor, K. E., R. J. Stouffer, and G. A. Meehl, 2012: An Overview Of Cmip5 And The Experiment Design. *Bulletin of the American Meteorological Society*, **93,** 485-498.

Tjiputra, J. F., and Coauthors, 2013: Evaluation of the carbon cycle components in the Norwegian Earth System Model (NorESM). *Geoscientific Model Development*, **6,** 301-325.

van Vuuren, D. P., and Coauthors, 2011: The representative concentration pathways: an overview. *Climatic Change*, **109,** 5-31.

Vancoppenolle, M., L. Bopp, G. Madec, J. Dunne, T. Ilyina, P. R. Halloran, and N. Steiner, 2013: Future Arctic Ocean primary productivity from CMIP5 simulations: Uncertain outcome, but consistent mechanisms. *Global Biogeochemical Cycles*, **27,** 605-619.

Vichi, M., and Coauthors, 2011: Global and regional ocean carbon uptake and climate change: sensitivity to a substantial mitigation scenario. *Climate Dynamics*, **37,** 1929-1947.

Figure Captions

Figure 1. Time series of global mean surface stratification, SST and SSS for historical run and RCP8.5 over 1850-2100. Surface stratification is defined as the density difference between 200m and the surface. Red square indicates observations from the WOA2009 data.

Figure 2. The spatial pattern for changes in stratification intensity changes between the 1990s and the 2090s.

Figure 3. Time series of nitrate (NO_3), phosphate (PO_4), silicate (SiO_4) and dissolved iron (dFe) concentrations (0-100 m) are shown for 1850-2100. Red square indicates WOA2009 global mean values.

Figure 4. Time series are displayed of mean changes (in percent) relative to the 1990s for (a) NO_3, (b) PO_4, (c) SiO_4 and (d) dFe (0-100m) during 1850-2100.

Figure 5. Time series of global mean net primary production, export production, and the particle export ratio over 1850-2100 are shown for each model.

Figure 6. Time series are displayed of the percent changes in net primary production, export production, and the particle export ratio, and stratification over the period 1850-2100 (each relative to their 1990s means).

Figure 7. Relationships are shown between the relative percent change in surface stratification with climate and the relative change in several biogeochemical variables including net primary production (NPP) (a), silicate (b), nitrate (c), phosphate (d), export production (EP) (e), the fraction of NPP by diatoms (g). EP is plotted against the change in the fraction of NPP by diatoms (g) and against the change in NPP (h). All changes are relative to the 1990s and plotted over 1850-2100. These time series are derived from global annual mean data.

Figure 8. The fraction of total NPP by diatoms for the 1990s is shown for each model (data for NorESM not available).

Figure 9. The percent change in NPP by diatoms between the 2090s and the 1990s.

Figure 10. The mean particle export ratio for the 1990s is shown for each model.

Figure 11. The percent change in the particle export ratio (pe-ratio) between the 2090s and the 1990s).

Figure 12. The stratification bias for the 1990s is plotted for each model versus the relative changes in NPP (a), EP (b), and stratification (C) with climate change (2090s – 1990s).

Supplementary Figure Captions

Figure S1. Mean vertical profiles are shown for density (a), temperature (c) and salinity (e) for the 1990s. Changes between the 2090s-1990s are shown in (b), (d) and (f), for the same variables. Solid black line denotes WOA2009 data.

Figure S2. Fractional contribution of temperature to the stratification change from the 1990s to the 2090s is shown for each model.

Figure S3. Mean NO_3 concentrations in the first 100 m for the1990s, R-squared and logarithmic transformed root mean square error (RMSE) are indicated relative to observations from the WOA2009.

Table 1: A brief description of components of the ESMs used in this study, for atmosphere and ocean components, the number of levels in the vertical is indicated by 'lev' and then the horizontal resolution is indicated in degrees, vertical coordinates of the ocean and biogeochemical components are indicated by Z (geopotential) or I (isopycnal).

Model	Resolution		Vertical coordinate	Reference	Biogeochemical component	References
	Atmosphere	Ocean				
GFDL-ES2M	24 lev,2.5/2.0°	50 lev,0,3-1°	Z	Dunne et al. (2013a)	TOPAZ2	Dunne et al. (2013b)
GFDL-ES2G	24 lev,2.5/2.0°	50 lev,0,3-1°	Z+I	Dunne et al. (2013a)	TOPAZ2	Dunne et al. (2013b)
MPI-ESM-LR	47 lev,1.9°	40 lev, 1.5°	Z	Giorgetta et al. (2013)	HAMOCC5.2	Ilyina et al. (2013)
MPI-ESM-MR	47 lev,1.9°	40 lev, 0.4°	Z	Giorgetta et al. (2013)	HAMOCC5.2	Ilyina et al. (2013)
IPSL-CM5A-LR	39 lev,1.9/3.8°	31 lev, 0.5-2°	I	Dufresne et al. (2013)	PISCES	Aumont and Bopp (2006)
IPSL-CM5A-MR	39 lev,1.2/1.9°	31 lev, 0.5-2°	I	Dufresne et al. (2013)	PISCES	Aumont and Bopp (2006) Seferian et al (2013)
HadGEM2-ES	38 lev,1.2/1.9°	40 lev, 0.3-1°	Z	Jones et al (2011) Collins et al. (2011)	Diat-HadOCC	Palmer and Totterdell (2000)
CESM-BGC	26 lev,1.25/0.94°	60 lev, 1.125° /0.27-0.53°	Z	Gent et al. (2011) Lindsay et al. (2013)	BEC	Moore et al. (2004) Doney et al (2009)
NorESM1-ME	26 lev,1.9°	70 lev, 1.5°	I	Bentsen et al. (2013)	HAMOCC5.1	Tjiputra et al. (2013)

Table 2: A brief description of the marine biogeochemical components included in the ESMs. Nutrients limiting phytoplankton growth, the number of explicit phytoplankton groups, the number of explicit zooplankton groups, representation of heterotrophic bacteria, the use of fixed fixed (Redfield: R) or variable (V) ratios for organic matter production, and Q_{10} for temperature dependency of biogeochemical processes (autotrophic/heterotrophic) are indicated.

Model	Nutrients	Phytoplankton	Zooplankton	Organic Materia Ratio	Q_{10}
TOPAZ2	5 ($NO_3, NH_4, PO_4, SiO_4, F_e$)	3 (diatom, eukaryotes, small diazotrophs)	1	R(C:N) $V(P, S_i, Chl, F_e)$	1.88
HAMOCC5.2	3 (NO_3, F_e, PO_4)	1 (separated into, diatoms and calcifiers)	1	R(C:N:P:Fe)	1.88
HAMOCC5.1	3 (NO_3, F_e, PO_4)	1 (separated into, diatoms and calcifiers)	1	R(C:N:P:Fe)	1.88
PISCES	5 ($NO_3, F_e, PO_4, NH_4, SiO_4$	2 (diatoms and, nanophytoplankton)	2 (micro and meso-)	R(C:N:P) $V(S_i, Chl, F_e)$	1.88/2.14
Diat-HadOCC	4 (NO_3, F_e, NH_4, SiO_4	2 (diatoms and, non-diatom)	1	R(C:N) $V(S_i, F_e)$	none
BEC	5 ($NO_3, NH_4, PO_4, SiO_4, F_e$)	3 (diatom, nano-, phyto, diazotrophy)	1	R(C:N:P) $V(S_i, Chl, F_e)$	2.0

Table 3: Global average of sea surface temperature (SST), sea surface salinity (SSS), nitrate (NO_3), phosphate(PO_4), NPP, EP, particle export ratio (pe-ratio), stratification index (SI) defined as density difference between 200 m and the surface and NPP by diatom (%) for the 1990s and 2090s. Observed estimates for the 1990s are obtained from WOA09 data for SST, SSS, nitrate and phosphate, from Carr et al. (2006) for NPP.

	SST		SSS		NO3(0-100m)		PO4(0-100m)		NPP		EP		pe-ratio		SI		%Diat	
	°C		psu		mmol/m^3		mmol/m^3		PgC/yr		PgC/yr		%		kg/m^3		%	
	1990s	2090s	1990s	2090s	1990s	2090s	1990s	2090s	1990s	2090s	1990s	2090s	1990s	2090s	1990s	2090s	1990s	2090s
Observations	18.3		34.57		6.73		0.63		50.0						1.81			
GFDL-ESM2G	18.5	20.4	34.06	33.98	6.65	6.10	0.66	0.58	57.8	57.5	4.40	4.10	7.60	7.02	2.35	2.75	10.7	9.7
GFDL-ESM2M	18.8	20.6	34.32	34.24	8.67	8.22	0.58	0.55	77.6	78.1	6.54	6.06	8.44	7.77	1.95	2.31	9.4	8.8
MPI-ESM-LR	18.3	20.7	34.38	34.23	7.20	6.61	0.57	0.50	45.7	41.6	7.23	6.05	15.84	14.56	1.88	2.41	78.7	80.1
MPI-ESM-MR	18.4	20.9	34.41	34.25	6.96	6.45	0.53	0.47	47.9	43.0	6.56	5.67	13.70	13.20	1.97	2.50	91.1	92.2
IPSL-CM5A-LR	17.7	21.0	34.52	34.43	5.62	4.81	0.43	0.36	28.9	27.0	5.96	4.87	20.61	18.05	2.05	2.63	23.1	20.3
IPSL-CM5A-MR	18.2	21.5	34.42	34.33	5.82	4.99	0.45	0.38	31.8	29.3	6.33	5.28	19.94	17.99	2.12	2.75	22.0	19.7
HadGEM2-ES	18.3	21.5	34.06	33.83	6.56	5.82	0.44	0.36	34.5	29.7	4.77	4.10	13.82	13.79	2.45	3.18	58.8	58.3
CESM1-BGC	19.0	21.4	34.23	34.18	7.60	6.56	0.71	0.54	54.2	52.1	6.97	6.26	12.86	12.03	2.25	2.63	35.7	33.2
NorESM1-ME	18.1	20.2	34.34	34.26	7.01	6.18	0.60	0.51	38.6	35.3	6.81	6.18	17.64	17.52	1.74	2.01		
Model Mean	18.4	20.9	34.30	34.19	6.90	6.19	0.55	0.47	46.3	43.7	6.17	5.39	14.49	13.55	2.08	2.57	41.2	40.3

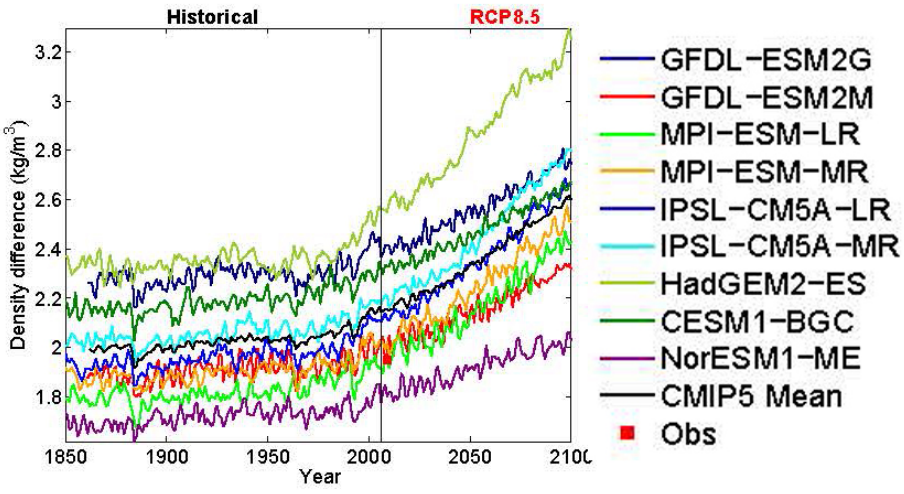

(a) Stratification

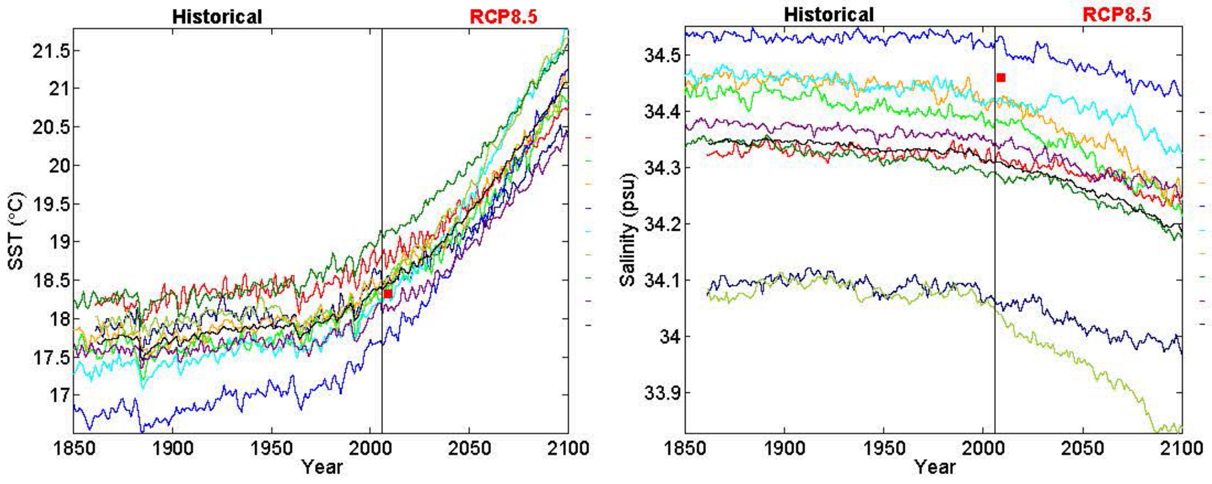

(b) SST (c) SSS

Fig. 1: Time series of global mean stratification, SST and SSS for historical run and RCP8.5 over 1850-2100. Stratification is defined as the density difference between 200 m and the surface. Red square indicates observations from the WOA2009 data.

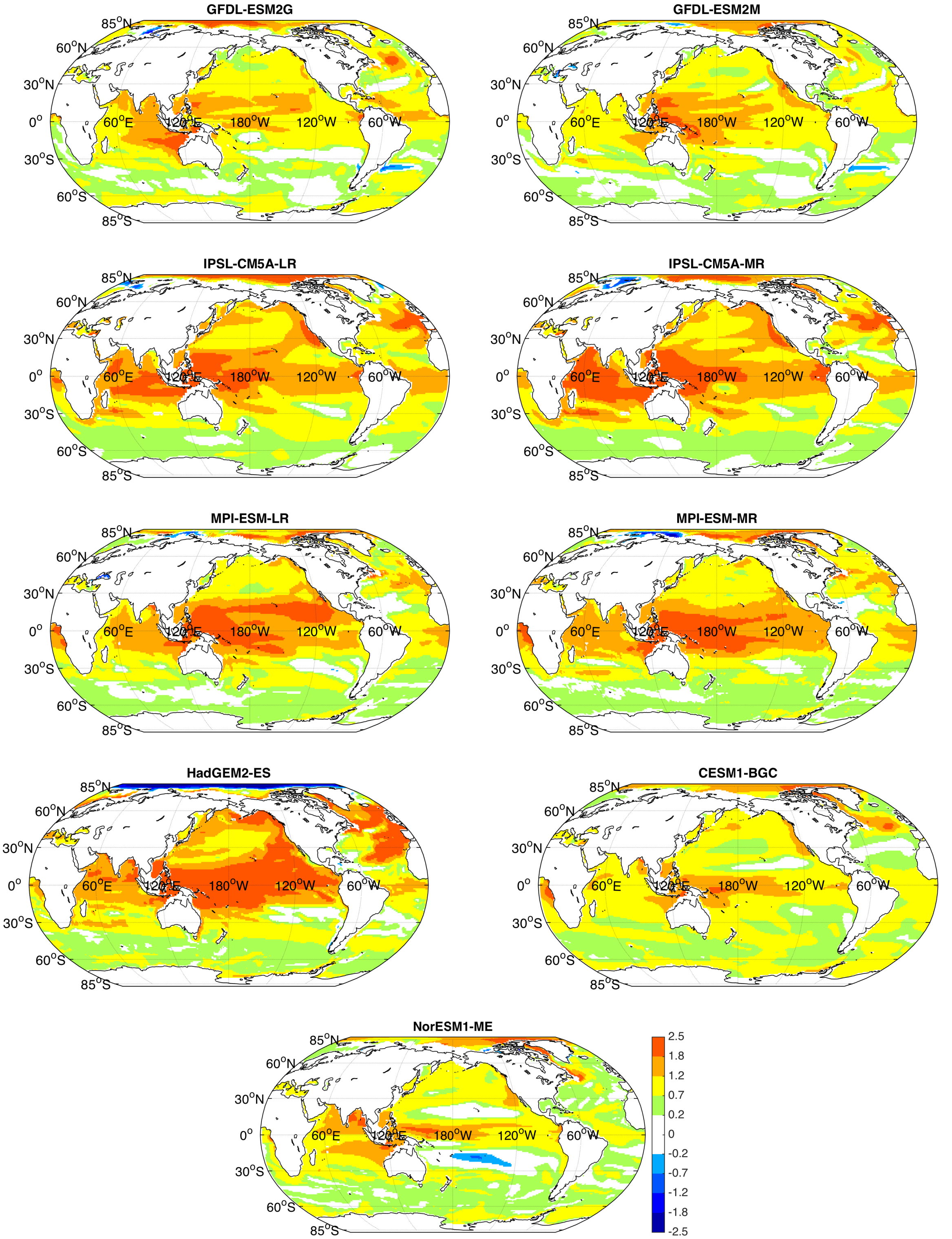

Fig. 2: The change in stratification (kg/m^3) from the 1990s to the 2090s is shown for each model.

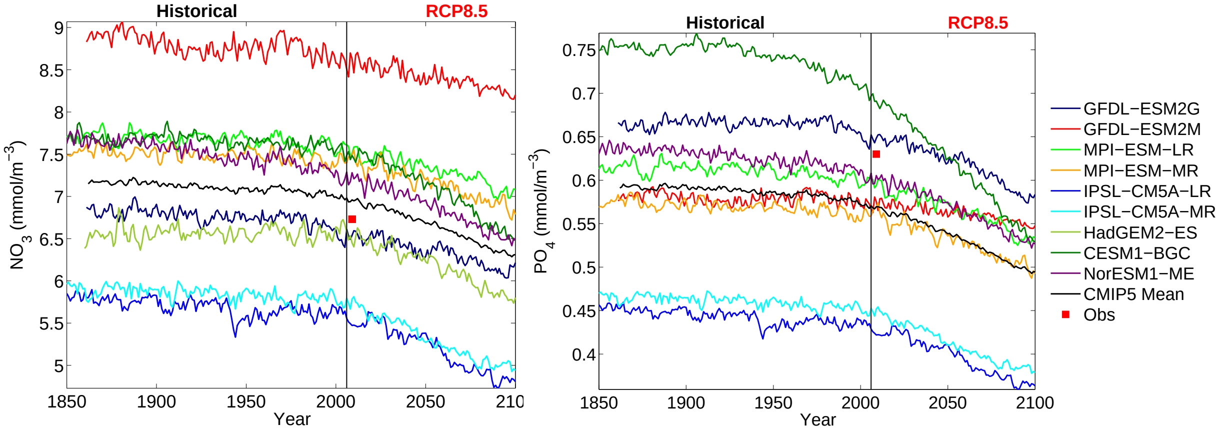

(a) NO$_3$ (b) PO$_4$

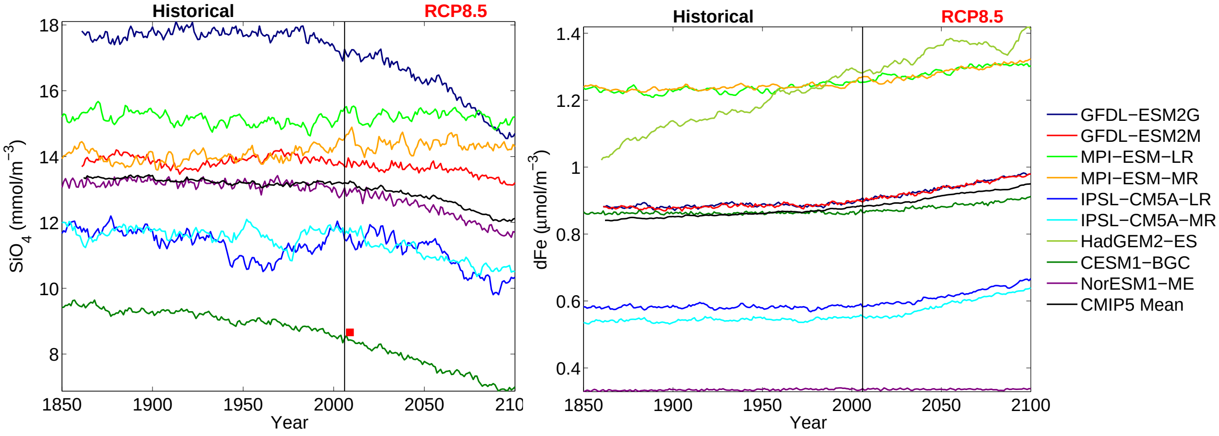

(c) SiO$_4$ (d) dFe

Fig. 3: Time series of mean nitrate (NO$_3$), phosphate (PO$_4$), silicate (SiO$_4$) and dissolved iron (dFe) concentrations (0-100 m) are shown for 1850-2100. Red square indicates WOA2009 global mean values.

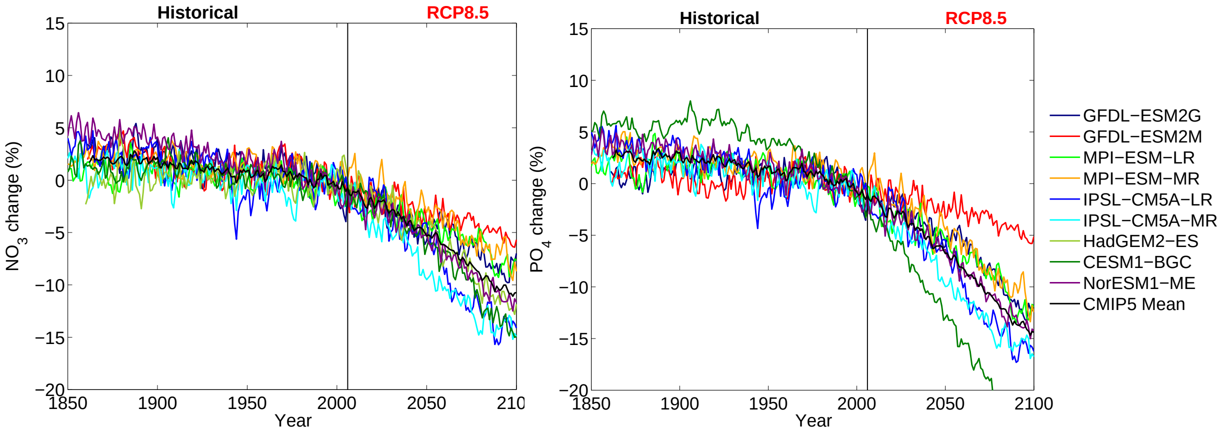

(a) NO3 change (b) PO4 change

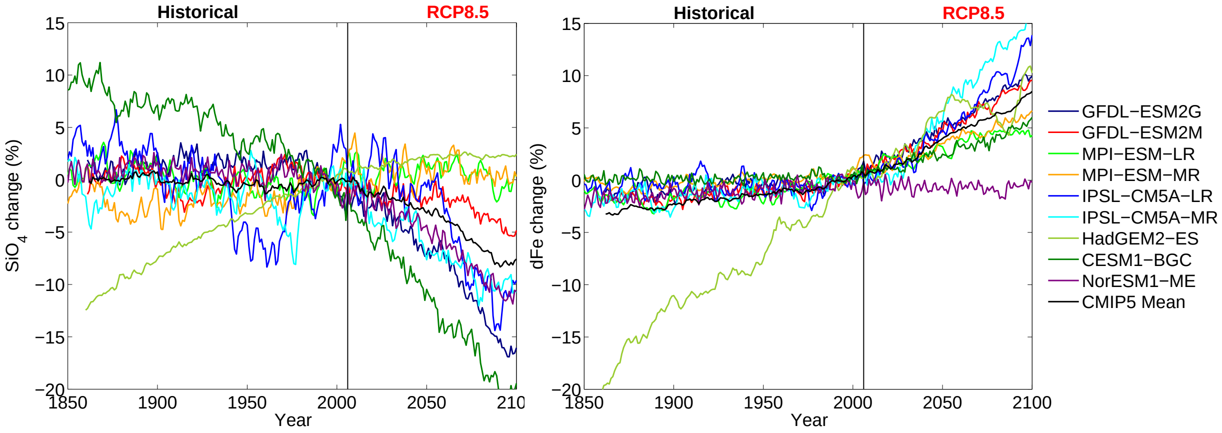

(c) SiO4 change (d) dFe change

Fig. 4: Time series are displayed of mean changes (%) relative to the 1990s for (a)NO_3, (b)PO_4, (c)SiO_4 and (d) dFe (0-100m) during 1850-2100.

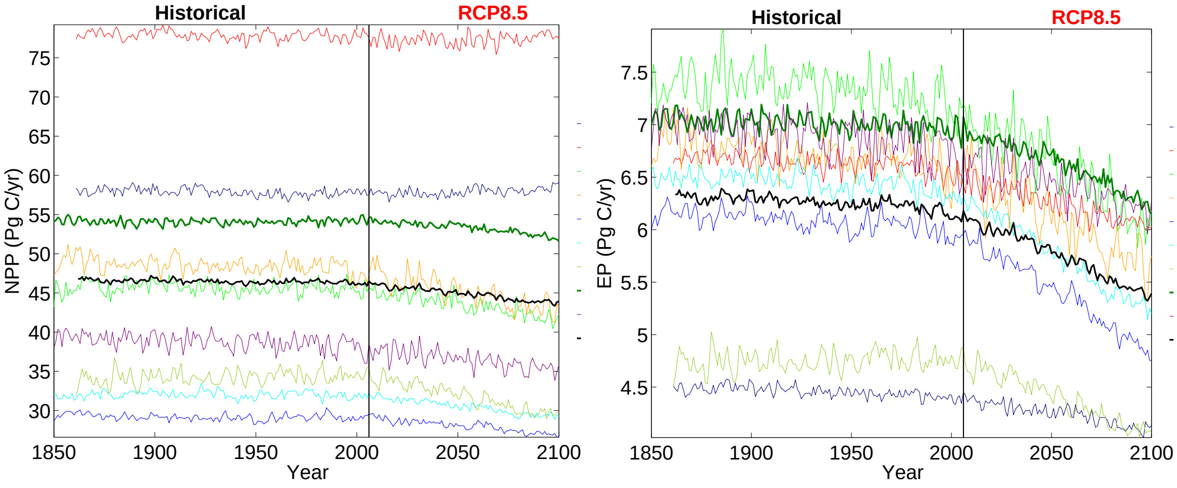

(a) NPP

(b) EP

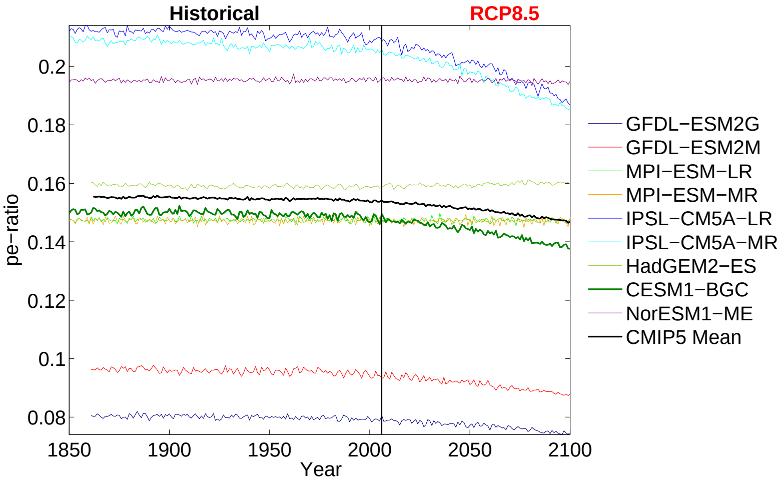

(c) pe-ratio

Fig. 5: Time series of global mean NPP, EP, and pe-ratio over 1850-2100 are shown for each model.

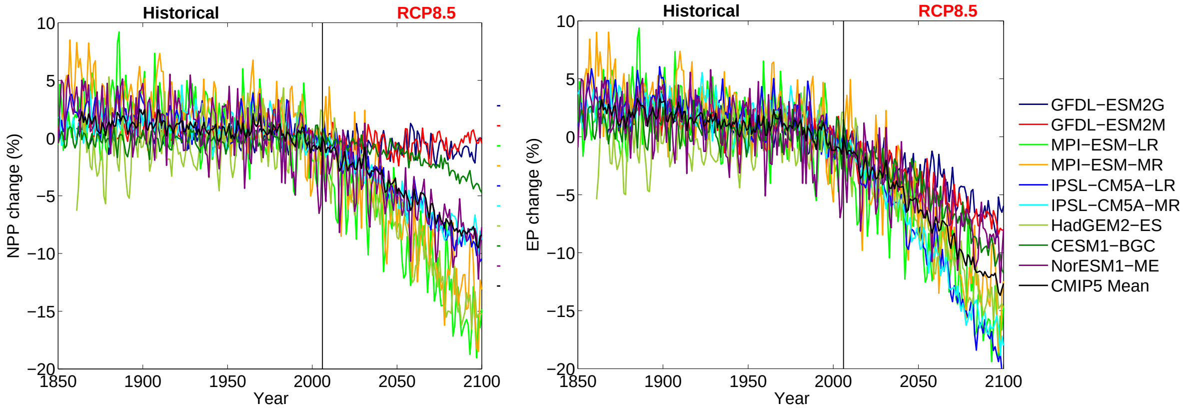

(a) NPP change (b) EP change

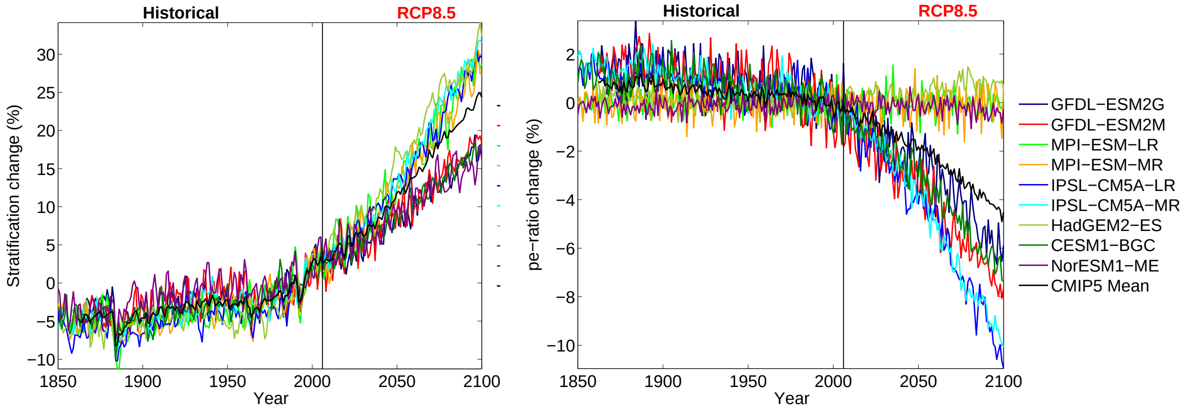

(c) SI change (d) pe-ratio change

Fig. 6: Time series are displayed of the percent changes in NPP, EP, pe-ratio and stratification over the period 1850-2100 (each relative to the 1990s means).

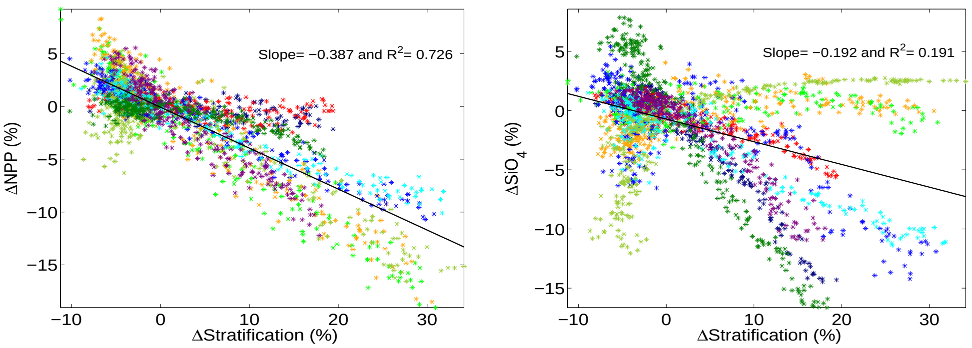

(a) ΔSI vs ΔNPP (b) ΔSI vs ΔSiO_4

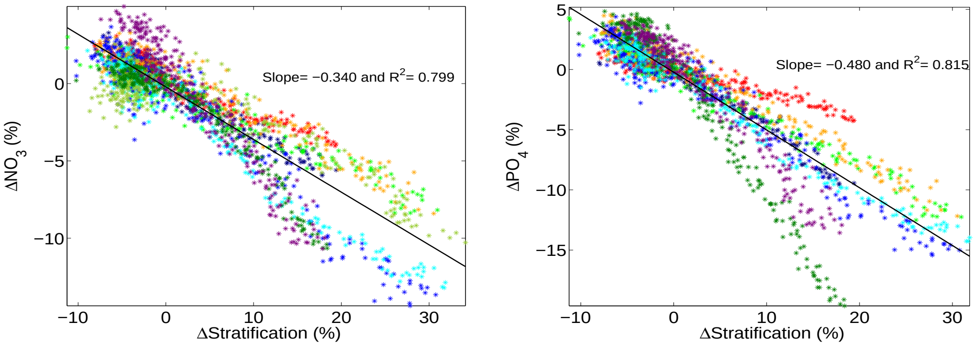

(c) ΔSI vs ΔNO_3 (d) ΔSI vs ΔPO_4

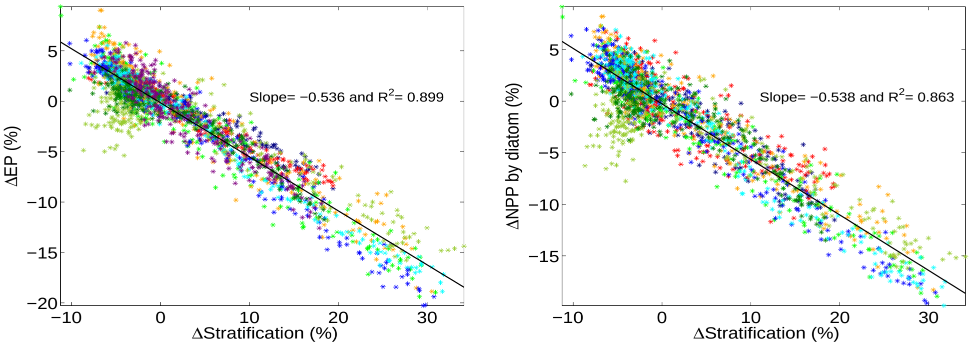

(e) ΔSI vs ΔEP (f) ΔSI vs ΔNPP by diatom

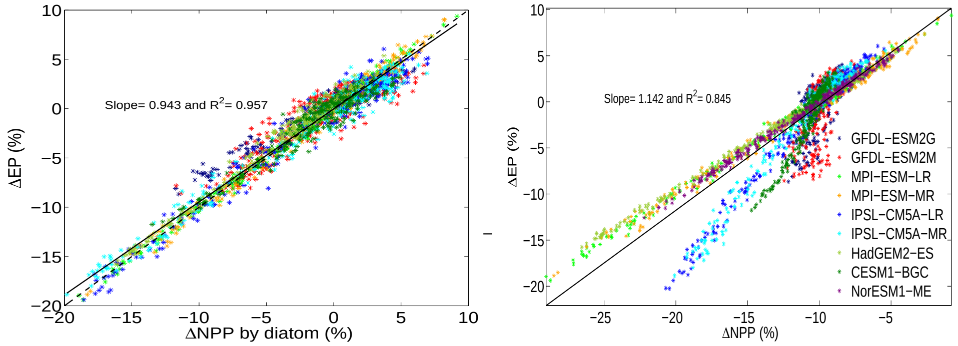

(g) ΔNPP by diatom vs ΔEP (h) ΔNPP vs ΔEP

Fig. 7: Relationship are shown between the relative percent change in the stratification index (SI) with climate and the relative changes in several biogeochemical variables including NPP (a), silicate (b), nitrate (c), phosphate (d), EP (e), the fraction of NPP by diatoms (f). EP is plotted against the change in the fraction of NPP by diatoms (g) and against the change in NPP (h). All changes are relative to the 1990s and plotted over 1850-2100. Results are derived from global annual mean data .

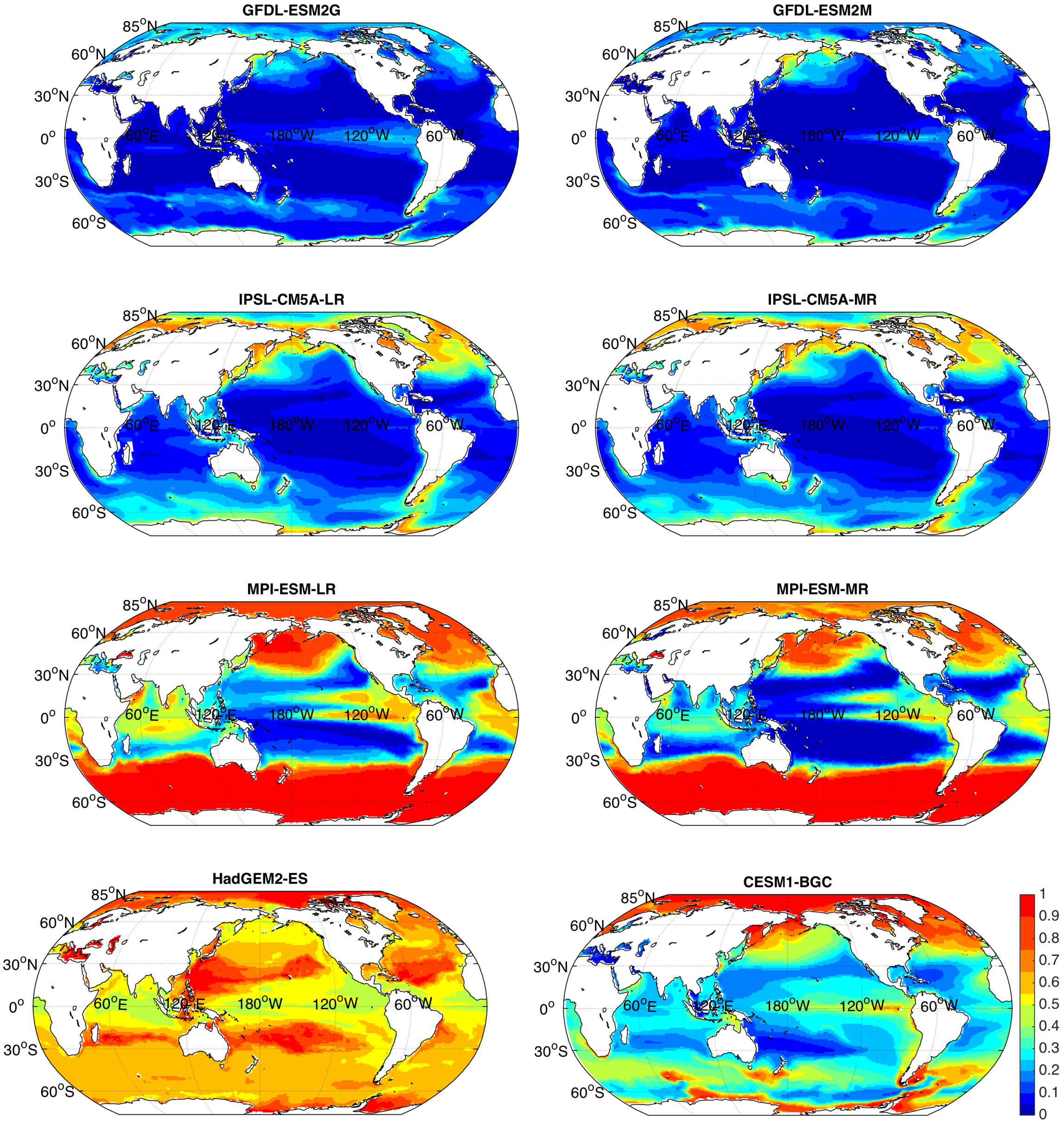

Fig. 8: The fraction of total NPP by the diatom for the 1990s is shown for each model (data for NorESM not available).

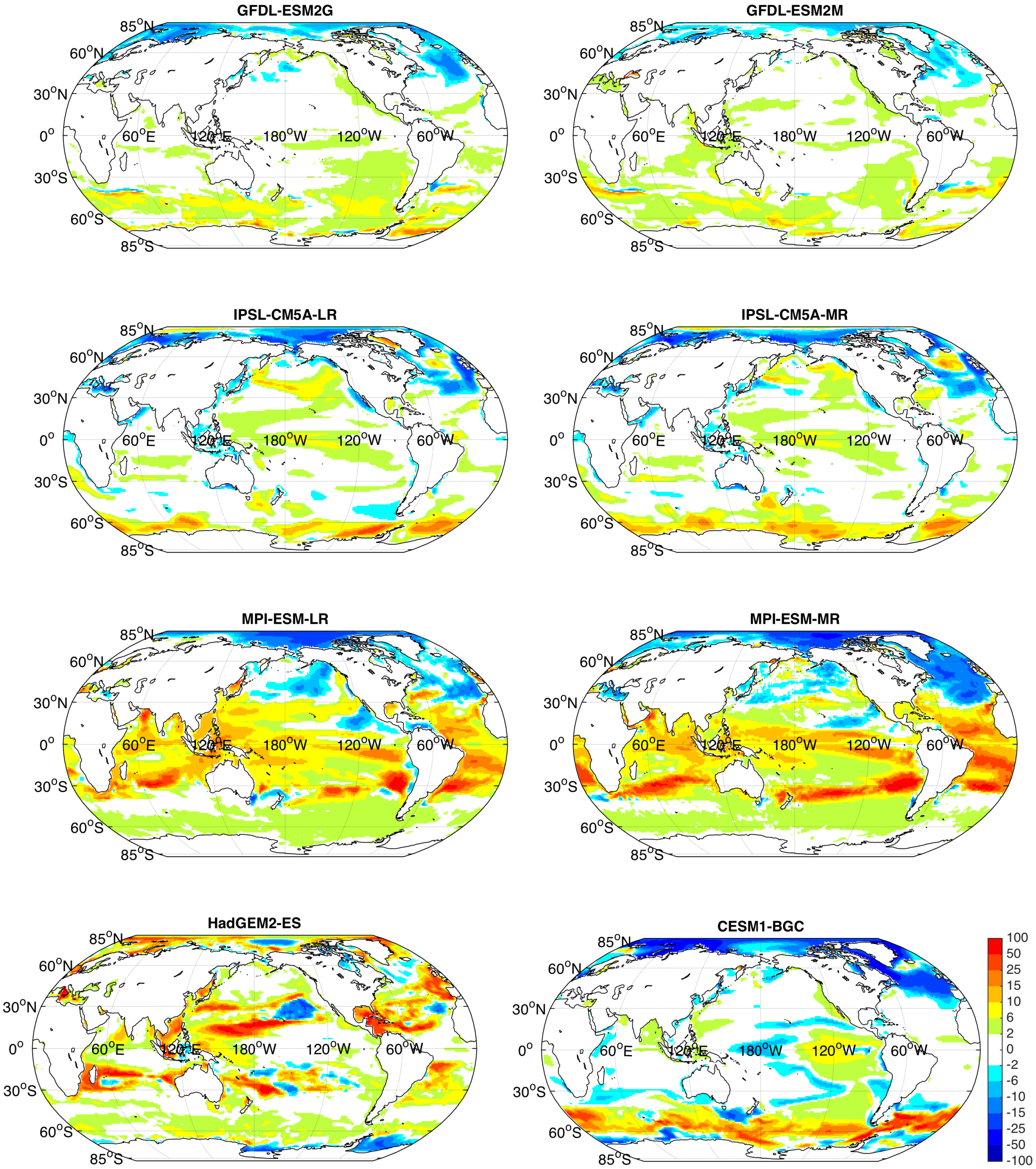

Fig. 9: The percent change in total NPP by diatoms between the 2090s and the 1990s.

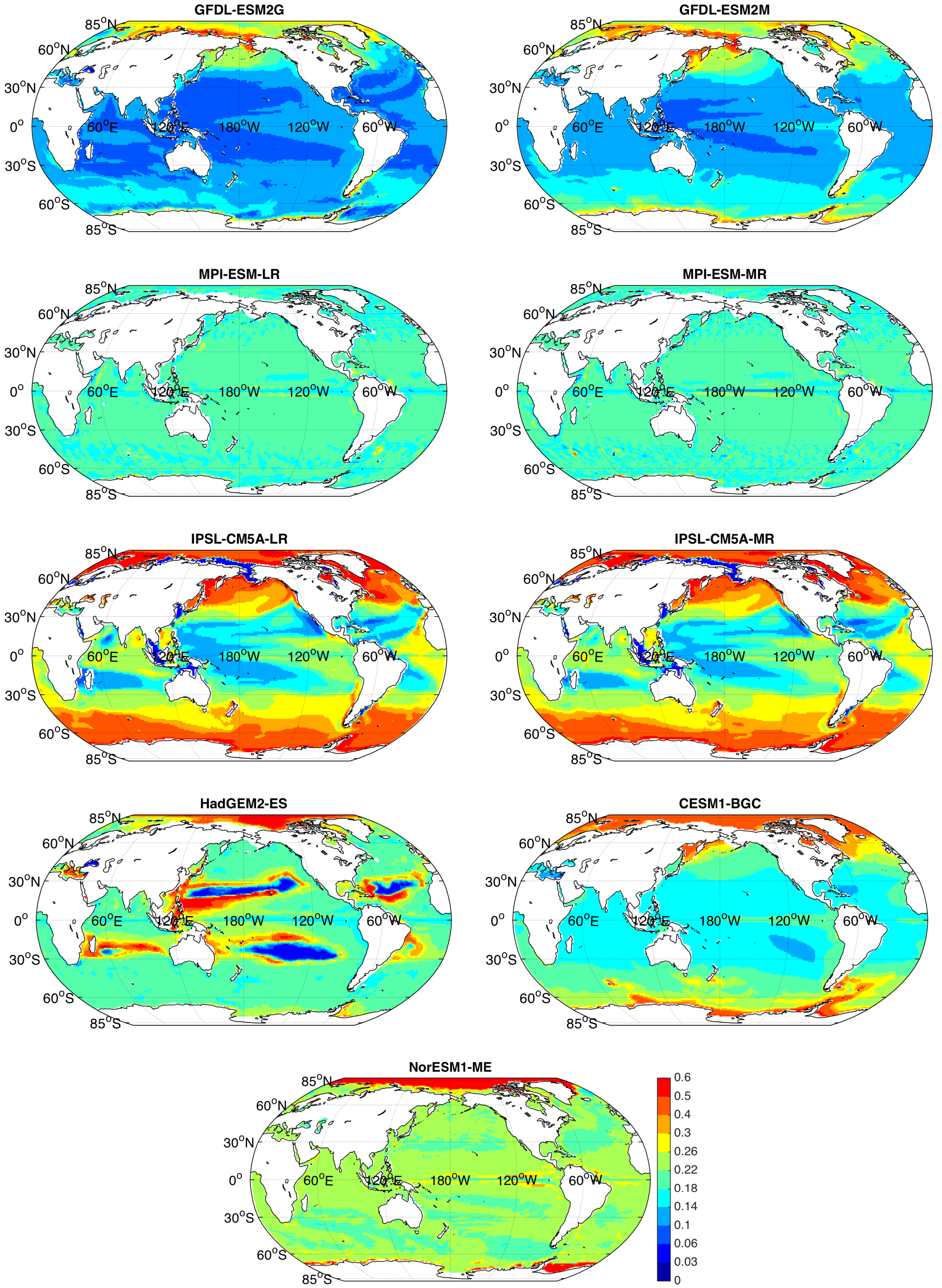

Fig. 10: The mean particle export ratio (pe-ratio) for the 1990s is shown for each model.

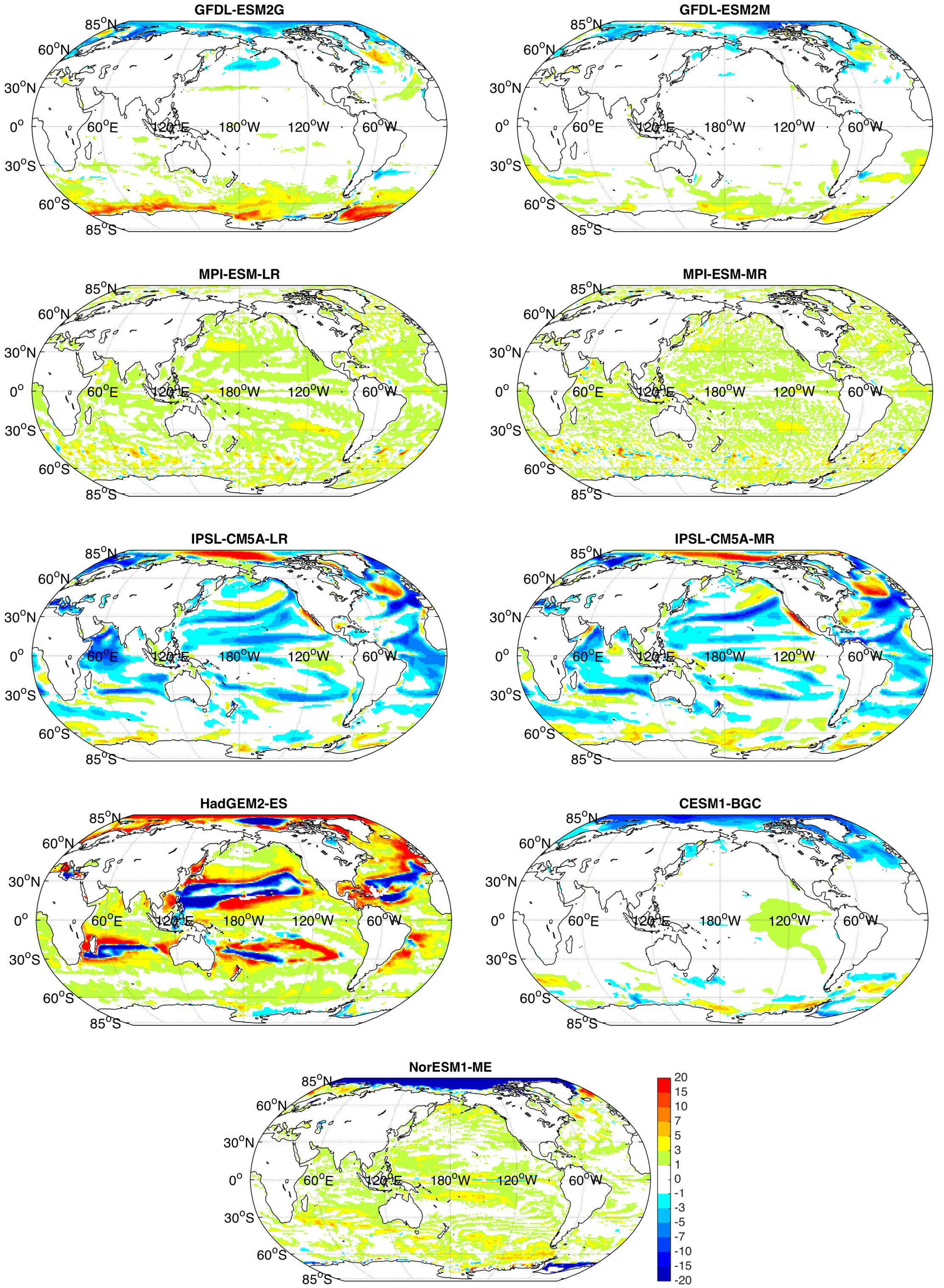

Fig. 11: The percent change in particle export ratio (pe-ratio) between the 2090s and the 1990s.

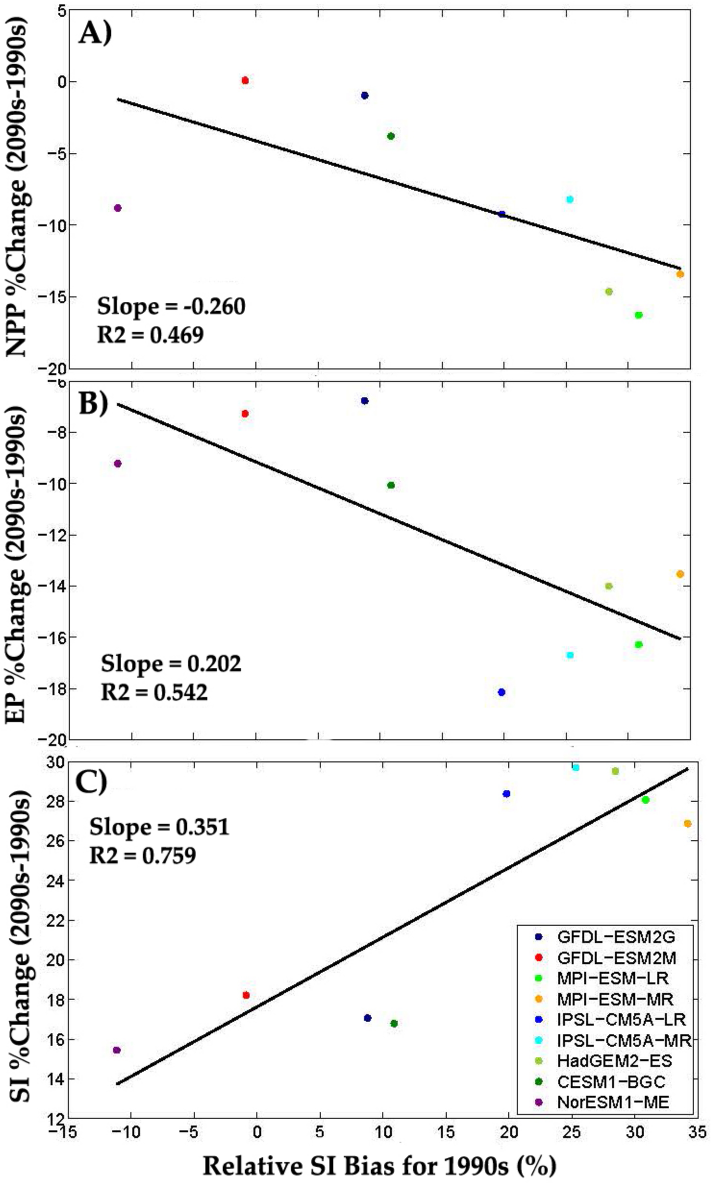

Fig. 12: The stratification bias for the 1990s is plotted for each model versus the relative changes in NPP (a), EP (b), and pe-ratio (c) with climate change (2090s-1990s).

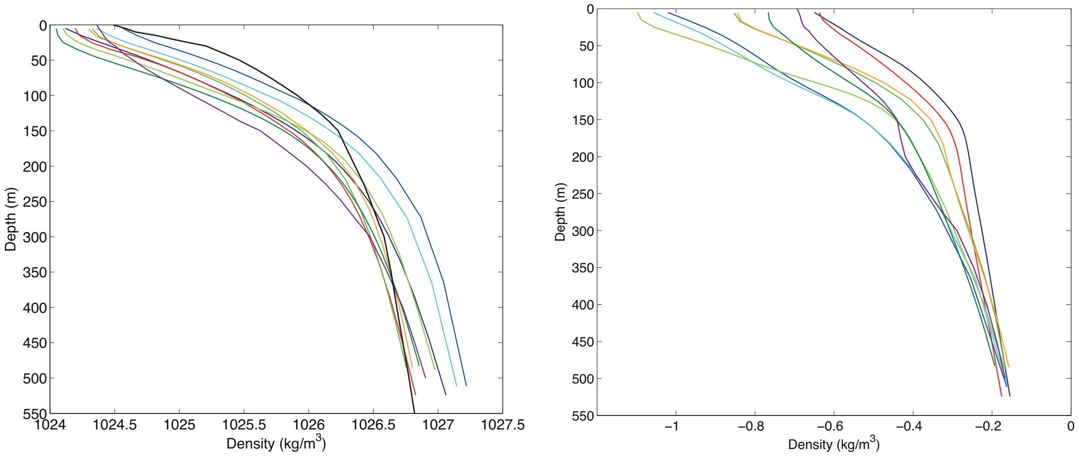

(a) density profile (b) density change

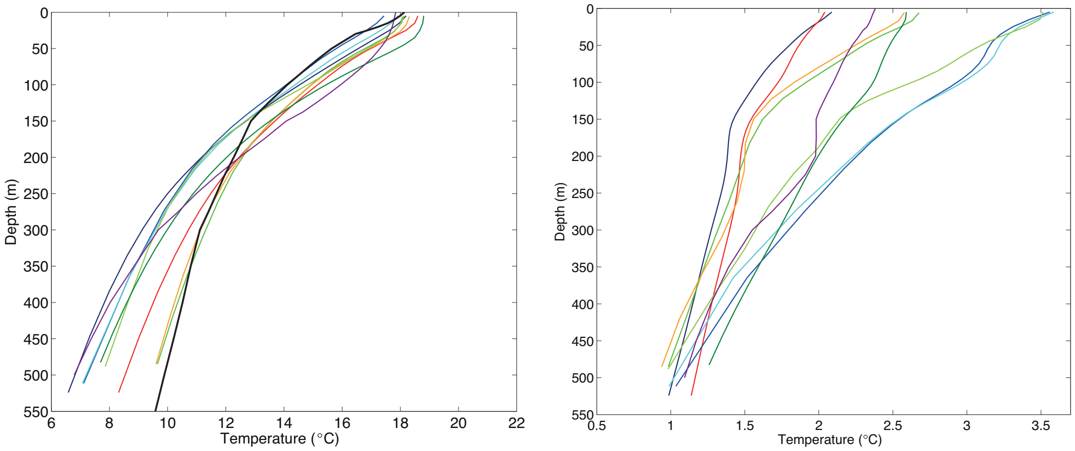

(c) temperature profile (d) temperature change

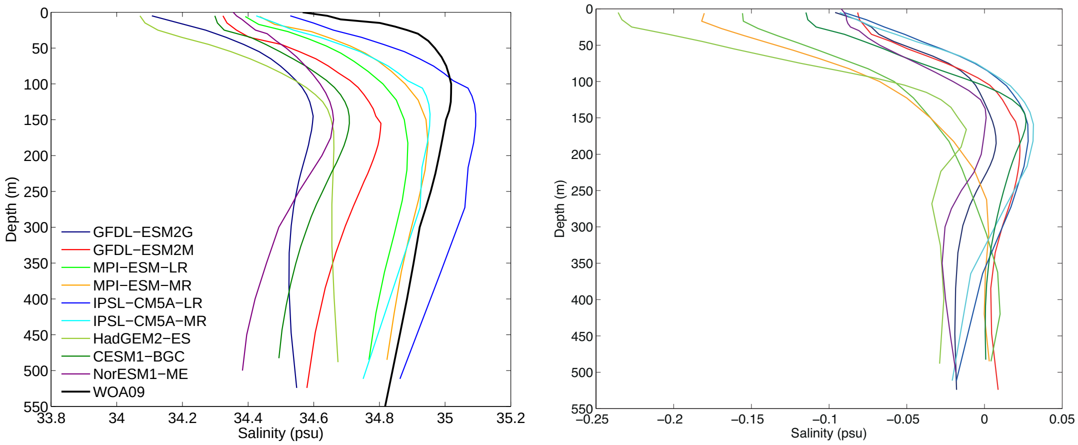

(e) salinity profile (f) salinity change

Figure S1. Mean vertical profiles are shown for density (a), temperature (c) and salinity (e) for the 1990s. Changes between the 2090s and1990s are shown in (b), (d) and (f), for the same variables. Solid black line denotes WOA2009 data.

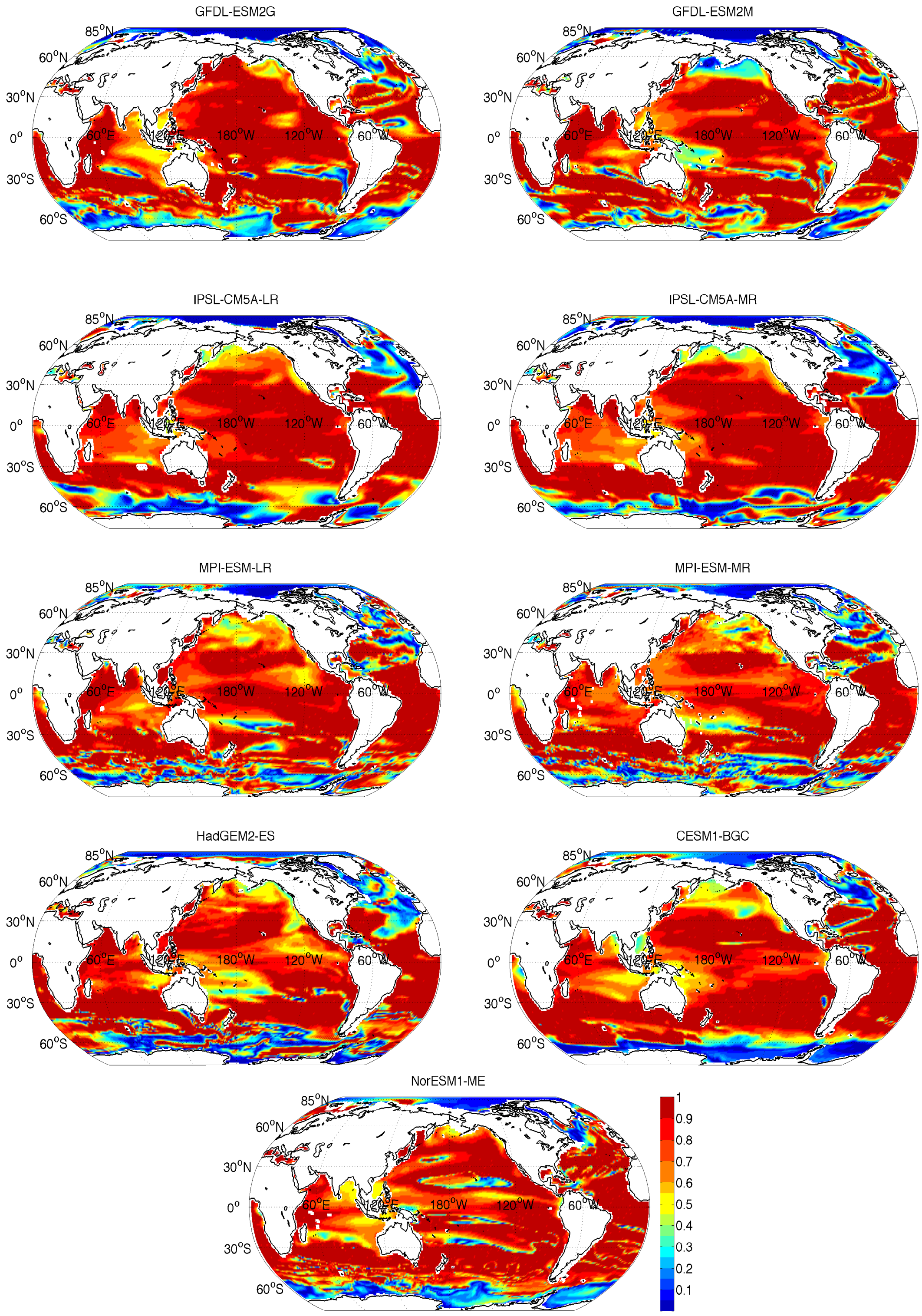

Figure S2. Fractional contribution of temperature to the stratification change from the 1990s to the 2090s is shown for each model.

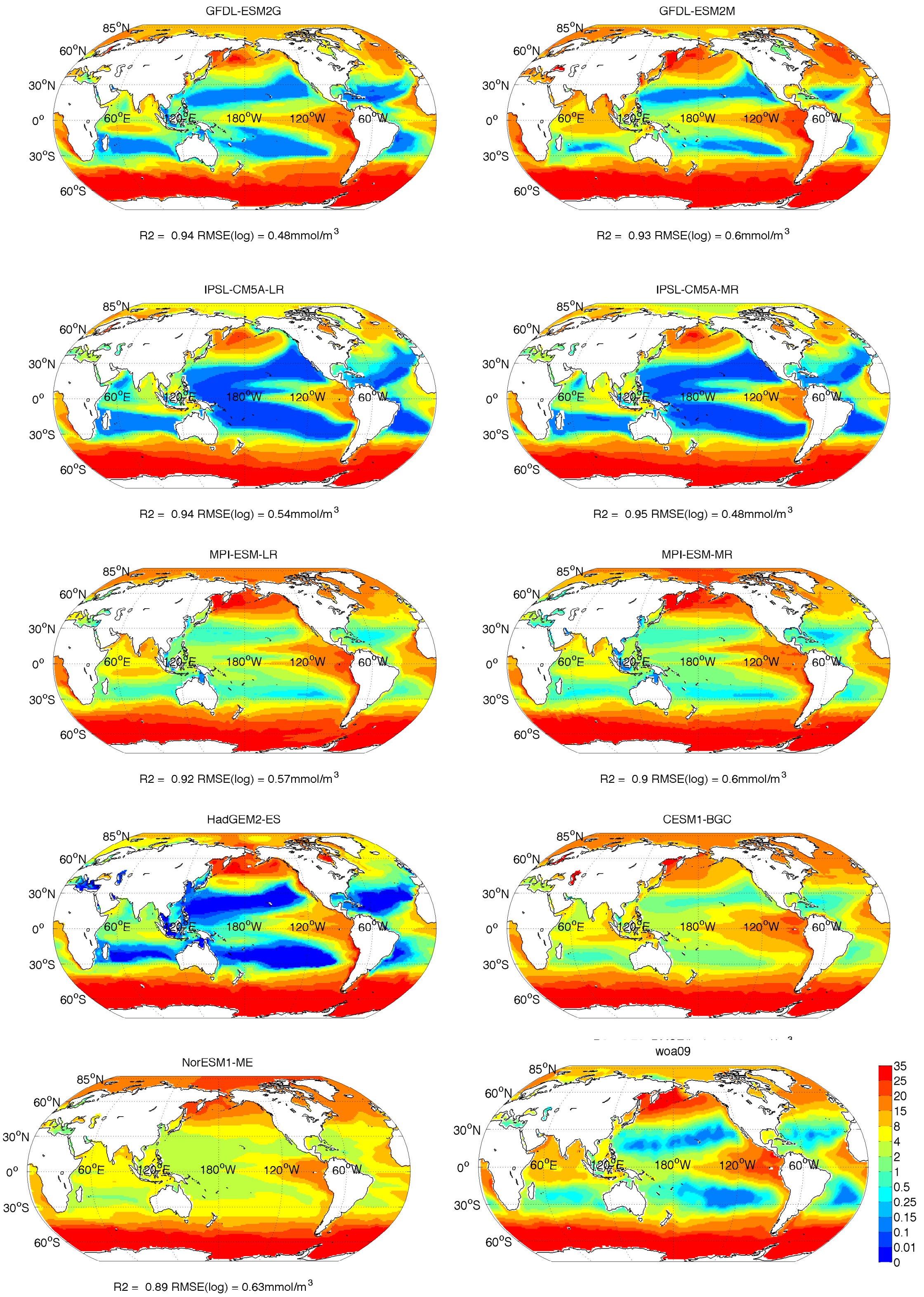

Figure S3. Mean nitrate concentrations in the first 100 m for the 1990s, R-squared and logarithmic transformed root mean square error (RMSE) are indicated relative to observations from the WOA2009.